MODELLING OF PISTON RINGS & BLOW-BY IN HYDROGEN ENGINE

M.Tech. Thesis

By
RUPESH KUMAR



Department of Mechanical Engineering
INDIAN INSTITUTE OF TECHNOLOGY INDORE
May,26

MODELLING OF PISTON RINGS & BLOW-BY IN HYDROGEN ENGINE

A THESIS

Submitted in partial fulfillment of the requirements for the award of the degree
of
Master of Technology

by
RUPESH KUMAR



Department of Mechanical Engineering
INDIAN INSTITUTE OF TECHNOLOGY INDORE
May,26

INDIAN INSTITUTE OF TECHNOLOGY INDORE

CANDIDATE'S DECLARATION

In this paper I submit my name as a post-graduate student who has completed the necessary coursework and examinations for a master's degree from IIT Indore. This project entitled; **Modelling of piston rings and blow-by in Hydrogen Engine** will fulfil part of the requirements to attain my master's degree. This report contains an authentic record of my work including research and documents created from the date of June 2025 to May 2026 when I will graduate from India under the supervision of Dr. Devendra Deshmukh, Professor, Department of Mechanical Engineering, IIT Indore.

I have not submitted my work for another master's or doctorate degree either inside or outside of India nor have I ever used my thesis or portions of my thesis for other degrees being pursued outside of this degree program.

Rupesh Kumar
26/05/2026

(Rupesh Kumar)

This is to certify that the above statement made by the candidate is correct to the best of my/our knowledge.

(prof. Devendra L. Deshmukh)

Mr. Rupesh Kumar has successfully given his M. Tech Oral examination held on 26-05-2026.

Signature of Supervisor of M. Tech. thesis

Date: 26-05-2026

Convener, DPGC

Date: 27-05-2026

DEDICATION

To my beloved parents,

whose silent sacrifices built the ground beneath my every step,
and whose unwavering faith in me became the fuel for this journey.

To my guide, Dr. Devendra Deshmukh,
who taught me that real engineering begins not with equations,
but with the courage to question and the discipline to persist.

And to every engineer who dares to look beyond the conventional —
may this work serve as a small flame in the larger pursuit
of a cleaner, hydrogen-powered world.

— Rupesh Kumar

IIT Indore, May 2026

ACKNOWLEDGEMENTS

I want to begin expressing my wholehearted gratitude to my advisor, **Dr. Devendra Deshmukh;** whose constant encouragement, expert guidance, and insightful suggestions throughout my two-year Master of Technology journey greatly contributed to the successful completion of my degree. He directly shaped the course of this project with his inspiration and guidelines.

Thanks go out to **Dr. Devashish Chorey** and **Mr. Arpit Joglekar** for their unyielding moral support, and to both for creating a shared atmosphere of excitement that allowed me to remain focused and complete this project. I would also like to thank Mr. Poojary Suraj, Brahmaiah jajula, and my fellow classmates for their friendship and accompanying me on this journey.

Finally, I want to thank my parents for their unwavering love, their blessings and their support, the foundation of my determination and endurance. I also thank everyone else who may have contributed to achieving the completion of this project in whatever way possible.

With Regards,

Rupesh Kumar

Abstract

The shift towards the development of low-carbon energy systems has led to the growing interest in hydrogen fueled internal combustion engines as a potential alternative energy source compared to traditional gasoline and diesel engines. Some of the environmental benefits of using hydrogen fueled internal combustion engines include the possibility of reduced carbon emissions. However, due to the low molecular weight and high diffusivity of hydrogen fuel, leakage is more likely compared to other conventional fuels. One of the major leakage sources in internal combustion engines is through the piston ring pack, which leads to the blow-by phenomenon. Excessive blow-by can lead to the loss of combustion pressure, reduced thermal efficiency, contamination of the lubricating oil, and the accumulation of hydrogen in the crankcase, which can lead to potential safety issues.

This study is concerned with the modeling and analysis of piston ring dynamics and blow-by in a hydrogen internal combustion engine using computational techniques. The comprehensive computational model is developed, including aspects of gas leakage modeling, piston ring dynamics, as well as thermal-structural analysis. The model is based on three main leakage sources in the piston ring assembly, including ring-liner clearance, piston ring end gap, as well as ring-groove side clearance. The mass conservation, energy balance, as well as gas flow equations are formulated to model the transient nature of hydrogen leakage in the compression chamber as well as the leakage chamber. Newton-Euler equations are used to model the dynamics of piston rings, influenced by contact forces as well as friction.

Transient simulations of the flow behavior have been carried out using ANSYS Fluent. The dynamic mesh technique has been used to simulate the piston motion based on crank angle variation. Hydrogen has been modeled as a compressible gas, and its thermophysical properties have been used in the simulation.

Besides the fluid flow simulation, thermal and structural analyses of the piston head have been carried out to study the temperature distribution, stress buildup, deformation, and fatigue effects. The simulation results have shown that the proposed methodology can be used to obtain a better understanding of the effects of gas leakage and piston ring behavior. The proposed methodology can be used to obtain valuable insights for designing piston rings for hydrogen internal combustion engines.

The simulation results show that the pressure in the cylinder is at its highest near the top dead center (TDC) of the piston, with a maximum pressure of around 67-70 bar at a speed of 1500 rpm. The blow-by flow is significantly dependent on the instantaneous combustion pressure. The highest blow-by occurs after reaching the peak pressure during the early expansion stroke. The maximum blow-by flow rate is found to be around 20.6 L/min, occurring at a crank angle of 90° after the top dead center. The simulation results show that pressure-driven flow is dominant in the leakage flow in the ring gap region, and blow-by occurs as the pressure in the cylinder reduces during the expansion stroke. The simulation results show that the proposed transient CFD-UDF coupling method can predict blow-by in hydrogen engines.

Table of Contents

ACKNOWLEDGEMENTS ..... **v**

Abstract ..... **vi**

Table of Contents ..... **viii**

List of Figures ..... **x**

Nomenclature ..... **xi**

Chapter 1: Introduction **1**

1.1 Background & History 1

1.2 Motivation 1

1.3 Problem Statement 2

1.4 Research Gap 3

1.5 Research Objectives 4

1.6 Need for the Present Study 5

1.7 Applications in Science and Industry 6

Chapter 2: Literature Review **7**

2.1 Early Analytical Models of Piston Ring Lubrication: 7

2.2 Hydrogen-Fuelled Internal Combustion Engines 8

2.3 Friction and Energy Loss Studies in Alternative Fuel Engines: 9

Chapter 3: Methodology **10**

3.1 Two-dimensional (2D) CFD Model of the Piston Assembly 10

3.2 Piston ring leakage model and used control equations: 11

3.3 Gas leakage equation: 12

3.4 Piston ring wear model: 14

3.5 Basics of CFD: 16

3.6 Simulation details: 17

3.7 Model simplification and assumptions: 19

3.8 Meshing Method: 20

3.9 Boundary conditions: 21

3.10 Dynamic Mesh: 24

Chapter 4: Results and Graphs **25**

4.1 Steady State thermal analysis of Piston Ring: 25

4.1.1 Total deformation of piston ring 25

4.1.2 Total Heat Flux of piston ring: 26
4.2 Static Structural analysis of Piston Head: 27
4.2.1 Total Deformation of piston head 27
4.2.2 Equivalent Elastic Strain of piston head: 28
4.2.3 Equivalent Von- mises Stress of piston head: 29
4.2.4 Safety Factor of piston head: 30
4.2.5 Life of Piston head of piston head: 32
4.2.6 Damage of Piston head: 33
4.2.7 Steady-State Thermal analysis of piston head 34
4.3 Transient thermal analysis of piston head: 35
4.3.2 Transient thermal analysis at cross- section: 36
4.3.3 Transient thermal analysis of Total heat Flux: 37
4.4. Piston Velocity graph at 4000 rpm: 39
4.4.1 Velocity contour for piston rings: 40
4.4.2 Combustion pressure Graph at 1500 rpm: 41
4.4.3 Pressure contour for piston rings: 43
4.4.4 Comparison between blow-by v/s crank angle graph: 45
Chapter 5: Conclusion 47
Chapter 6: Recommendations of Future Work 50
APPENDIX 51
Appendix A: Engine and Piston Assembly Specifications 51
Table A.1- Engine Geometry Parameters 51
Table A.2- Piston Ring Assembly Geometry 51
Table A.3- Thermal Boundary Conditions Used in Simulation 52
Appendix B: Material Properties 54
Table B.1- Piston Head Material Properties (Aluminium Alloy / Cast Steel).....54
Table B.2- Hydrogen Gas Properties Used in CFD Simulation 54
Appendix C: CFD Simulation Settings and Solver Parameters 56
Table C.1- ANSYS Fluent Solver Configuration 56
Table C.2- Blow-By Monitor Points.....57
Appendix D: Mesh Sensitivity Study 58
Chapter 7: References 59

List of Figures

Figure 1.1 Piston rings 5
Figure 2.1 Balance of forces on piston ring. 8
Figure 3.1 Leakage diagram of piston ring 12
Figure 3.2 Force analysis with the piston ring positioned at the bottom (a) and at the top (b). 15
Figure 3.3 Manual Meshing of piston rings 20
Figure 3.4 Required Boundary conditions parameters for thermal 23
Figure 3.5 Dynamic Meshing 24
Figure 4.1 Total deformation of piston ring 25
Figure 4.2 Total Heat Flux of piston ring 26
Figure 4.3 Total Deformation of piston head 27
Figure 4.4 Equivalent Elastic Strain of piston head 28
Figure 4.5 Equivalent Von- mises Stress of piston head 29
Figure 4.6 Safety Factor of piston head 30
Figure 4.7 Life of Piston head of piston head 32
Figure 4.8 Damage of Piston head 33
Figure 4.9 Steady-State Thermal analysis of piston head 34
Figure 4.10 Transient thermal analysis of piston head 35
Figure 4.10.1 Transient thermal analysis tabular data 35
Figure 4.11 Transient thermal analysis at cross- section 36
Figure 4.12 Transient thermal analysis of Total heat Flux 37
Figure 4.12.1 Transient heat flux analysis tabular data 38
Figure 4.13 Piston velocity v/s Crank angle graph at 4000 rpm. 39
Figure 4.14 Simulations of Velocity contour for piston rings. 40
Figure 4.15 Combustion pressure at 1500 rpm 41
Figure 4.16 Pressure results at selected crank angles. 43
Figure 4.17 Combustion pressure graph in bar (dark blue) and blow-by graph in l/min (sky blue). 45

Nomenclature

A. Latin Symbols

Symbol	Description	Unit
$\mathbf{A_{cut}}$	Leakage area at the piston ring cut (end gap)	m^2
$\mathbf{A_{heat}}$	Heat transfer area of control volume	m^2
$\mathbf{C_{cut}}$	Flow coefficient at the piston ring cut	–
D	Cylinder bore diameter	m
E	Total energy per unit volume	J/m^3
Fe	Elastic force of piston ring	N
Ff	Friction force on piston ring	N
$\mathbf{F_n}$	Normal contact force between ring and groove	N
$\mathbf{F_{ph}}$	Gas pressure force on piston-side face of ring	N
$\mathbf{F_{pl}}$	Gas pressure force on crankshaft-side face of ring	N
Fpm	Radial force from average gas pressure on ring–liner interface	N
$\mathbf{F_{pg}}$	Gas pressure force inside piston ring groove	N
$\mathbf{F_{pct}}$	Contact force from piston crown or land on ring	N
g	Gravitational acceleration vector	m/s^2
H	Hardness of the softer material (Archard model)	Pa
$\mathbf{h_{heat}}$	Convective heat transfer coefficient	$W/m^2 \cdot K$
I	Identity tensor	–
k	Thermal conductivity of gas	$W/m \cdot K$

K	Dimensionless Archard wear coefficient	–
k_{wear}	Wear coefficient in Archard's theory	–
m_{cut}	Mass flow rate through the ring end-gap cut	kg/s
m_r	Mass of piston ring	kg
p	Static pressure	Pa
p_{dn}	Downstream leakage chamber pressure	Pa
p_{up}	Upstream leakage chamber pressure	Pa
P_{dn}	Normalised downstream pressure (Archard)	Pa
P_{up}	Normalised upstream pressure (Archard)	Pa
Q_{heat}	Instantaneous heat transfer rate from control volume to wall	W
R_g	Specific gas constant of hydrogen	J/kg-K
S	Sliding distance (Archard wear model)	m
S_h	Energy source term	W/m^3
S_m	Mass source term	$kg/m^3 \cdot s$
T	Gas temperature	K
T_c	Control volume gas temperature	K
T_{up}	Upstream leakage chamber gas temperature	K
T_{wall}	Control volume wall temperature	K
U_{mean}	Mean piston velocity	m/s
u, v	Velocity components in x and y directions	m/s
V	Velocity vector	m/s
V_{wear}	Wear volume (Archard model)	m^3
W	Applied load (Archard wear model)	N
Z	Compressibility factor of upstream gas	–
a_r	Radial acceleration of piston ring	m/s^2

B. Greek Symbols

Symbol	Description	Unit
κ	Isentropic index (ratio of specific heats), C_p/C_v	–
η	Dynamic viscosity of gas	Pa-s
λ_c	Thermal conductivity of gas (CFD notation)	W/m-K
μ_c	Dynamic viscosity of gas (CFD notation)	Pa·s
ρ	Gas density	kg/m³
τ	Viscous stress tensor	Pa

C. Abbreviations & Acronyms

Abbreviations	Full form
ANSYS	Analysis System (commercial simulation software)
BC	Boundary Condition
CA	Crank Angle
CFD	Computational Fluid Dynamics
CNG	Compressed Natural Gas
FEA	Finite Element Analysis
FSI	Fluid–Structure Interaction
FVM	Finite Volume Method
IC / ICE	Internal Combustion Engine
IMEP	Indicated Mean Effective Pressure
ICEM CFD	Integrated Computer Engineering and Manufacturing CFD (meshing tool)
RPM	Revolutions Per Minute
TDC	Top Dead Centre
BDC	Bottom Dead Centre
UDF	User-Defined Function (ANSYS Fluent)
VOF	Volume of Fluid (multiphase model)

Chapter 1: Introduction

1.1 Background & History

Piston rings are utilized within internal combustion engines to seal off the combustion chamber, assist in controlling oil consumption and transferring heat from the engine. However, internal combustion engines still suffer from blow-by (the escape of gases through the ring pack) which is a significant problem facing internal combustion engines.[1]

Research into the dynamics of piston rings and blow-by began in the middle of the 20th century when analytical modelling of lubrication was first developed. The first attempt at hydrodynamics (i.e. hydrodynamic lubrication) of piston rings using the Reynolds lubrication equation occurred in 1959 when Furuhama proposed a transient model. Following this, further research continued the dynamics of piston rings and blow-by, to include transport of gases through the spaces between the rings, lubrication of the surfaces, and dynamic behaviour of the rings. Dowson and ruddy went on to improve the analysis of oil film and pull of the piston rings. [2]

The progression of computational strength has allowed many researchers to run numerous numerical simulations on the analysis of the dynamic behaviour of the piston rings. At first, 1-dimensional models were used to analyze flow rates of gases through the piston ring and only a later analysis of gas flow through the piston rings as well as the dynamic behaviour of the piston rings occurred using hydrodynamic lubrication and contact theories.[3]

1.2 Motivation

The growing awareness of climate change and greenhouse gas emissions has accelerated the pace of the search for cleaner forms of energy. Hydrogen is an excellent clean and high-energy-density fuel for IC engines. However, its low molecular weight and high diffusivity make the fuel prone to leakage, thereby increasing the blow-by through the piston rings.

Excessive hydrogen blow-by is an operational and safety problem. Hydrogen gas

leakage into the crankcase increases the risk of flammability, and the loss of combustion gases reduces the engine power and thermal efficiencies. To overcome these problems, there is a need for the development of an accurate prediction tool for hydrogen blow-by.

Most piston ring/blow-by models are designed for conventional IC engine fuels and do not consider hydrogen-specific properties such as diffusivity and viscosity. The piston ring/blow-by models are based on oversimplified gas flow, ring dynamics, lubrication, and structural coupling, thereby reducing the accuracy of the gas leakage prediction.

To overcome the shortcomings of the piston ring/blow-by models, the present study develops a CFD-based framework for the analysis of piston ring dynamics and hydrogen blow-by. The study uses gas leakage modeling, ring force analysis, and transient CFD simulations using the ANSYS Fluent software for the development of the framework for the prediction of hydrogen leakage and the design of piston rings for IC engines.

1.3 Problem Statement

Hydrogen-powered internal combustion engines have gained significant attention in recent times as a potential solution to combat the environmental problems of excessive carbon emissions in vehicles. Even though hydrogen-powered internal combustion engines have many advantages over traditional internal combustion engines, they face several problems associated with gas leakage through the piston ring pack, also called blow-by.

Hydrogen-powered internal combustion engines face a higher blow-by phenomenon than traditional gasoline or diesel-powered internal combustion engines because of the low molecular weight of hydrogen. Blow-by refers to the leakage of gases through the piston rings. The low molecular weight of hydrogen causes a higher leakage of gases, which may cause a loss of compression pressure, engine efficiency, and engine component wear. Blow-by gases entering the crankcase may also cause several safety issues because of the high flammability of

hydrogen. Hydrogen-powered internal combustion engines may cause a few problems because of the blow-by phenomenon.

Therefore, it is very important to predict blow-by to improve the efficiency of the engine. Most piston ring models and blow-by simulations have been developed for traditional gasoline or diesel-powered internal combustion engines. The thermophysical properties of hydrogen have not been considered in most piston ring models and blow-by simulations.

Most piston ring models and blow-by simulations have not been able to simulate blow-by because of the complex nature of the phenomenon. The complex nature of blow-by has not been considered in most piston ring models. Therefore, it is very important to develop a new advanced computational method to simulate blow-by.

1.4 Research Gap

There has been considerable research conducted on piston ring dynamics and blow-by prediction; however, there are still unfulfilled areas of research. Most of the past research has concentrated on standard internal combustion engines using standard fuel sources, such as gasoline/diesel. Very little research has focused on gas leakage behaviour for hydrogen.

The numerical simulations that are currently available are mostly based on simple one-dimensional or analytical approaches for simulating the gas flow through the piston ring package. Although these approaches are computationally cheap, the accuracy of the results obtained from these approaches might not be satisfactory for simulating the complex gas flow behaviour, pressure distribution, and transient effects that exist within the small crevices between the piston, piston rings, and cylinder liner.

Another research gap that needs to be fulfilled is that most of the research done so far has been focused on simulating the piston ring dynamics and gas flow behaviour separately rather than considering the coupled effects of the two. The piston ring dynamics, gas pressure forces, lubrication effects, and thermal deformation effects

are coupled and influence the blow-by behaviour. Moreover, no research has yet been done on using dynamic mesh CFD simulations coupled with piston motion simulations for simulating the hydrogen blow-by behavior.

Therefore, there is still a research gap that needs to be fulfilled for developing an integrated computational model for simulating the gas leakage behaviour, piston ring dynamics, and transient CFD simulations for hydrogen IC engines.

1.5 Research Objectives

The current goal of this research study is to develop a computational model for the analysis of the dynamics of the piston rings and the resulting blow-by in a hydrogen-powered internal combustion (IC) engine. The specific goals of the present study are:

To create a mathematical model for gas leakage through the piston ring set considering the thermophysical properties of hydrogen gas.

To identify the major gas leakage locations in the piston ring system, including the ring-liner clearance, ring end gap, and ring-groove side clearance.

To perform transient CFD simulations using the ANSYS Fluent code for the analysis of gas leakage through the piston ring set.

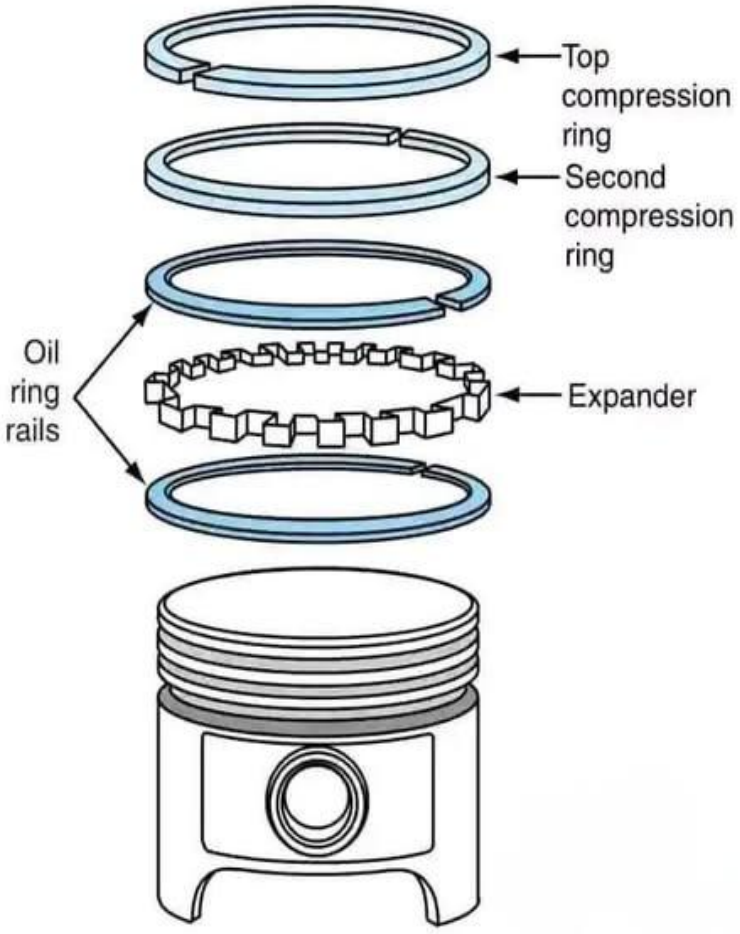


Figure 1.1 Piston rings

To apply the dynamic mesh approach for simulating the piston motion considering the crank angle variation. To analyze the pressure distribution, velocity fields, and blow-by mass flow rate during the engine cycle. To study the effects of engine operating conditions and piston ring dynamics on gas leakage characteristics. To provide design guidelines for improving the piston ring performance.

1.6 Need for the Present Study

There has been an increasing focus on the use of hydrogen as an alternate fuel in internal combustion engines with the advent of low-carbon energy systems. However, the low density and high diffusivity of hydrogen create problems in gas sealing. High rates of hydrogen leakage past the piston ring pack cause reduced engine efficiency, emission of unburned fuels, and safety concerns resulting from hydrogen accumulation in the crankcase. Most of the existing piston ring models

were developed for conventional fuels. However, these models do not consider the flow characteristics of hydrogen. Also, many studies were carried out using simple modelling techniques that do not consider the transient behavior of the piston rings. With recent advancements in computational fluid dynamics, it is now possible to simulate the complex processes in an engine more accurately.

Thus, it is necessary to develop a computational framework using CFD techniques to simulate hydrogen blow-by in an engine. This would help with designing improved piston rings that would result in better sealing efficiency, thus making internal combustion engines safer. This would reduce the cost of expensive experimental investigations.

1.7 Applications in Science and Industry

Research into the dynamics of piston rings and blow-by behaviour is an important area of scientific research that contributes to the advancement of scientific knowledge in the field of fluid mechanics, tribology, thermodynamics, and Multiphysics modelling in IC engines. The study of gas leakage through the piston ring pack allows the researcher to understand the complex interactions between gas flow, lubrication, friction, and heat transfer in the engine components.

Computational Fluid Dynamics (CFD) simulations are often applied in scientific research for the transient flow behaviour in the small crevices of piston assemblies. The simulations allow for detailed scientific study of the pressure distribution, velocity fields, and gas leakage from the combustion chamber to the crankcase. The study helps in the development of advanced theoretical models for piston ring lubrication, gas flow, and friction loss in the engine.

In automotive as well as energy industries, the piston ring sealing efficiency is seen to affect the efficiency, emission, durability, as well as fuel efficiency of the engines. Excessive blow-by causes loss of combustion pressure, excessive oil consumption, as well as hydrocarbon emission. Hence, it is of utmost importance to be able to accurately predict blow-by to create efficient as well as environmentally friendly engines.

Chapter 2: Literature Review

2.1 Early Analytical Models of Piston Ring Lubrication:

The piston ring-liner assembly plays an important role in the effectiveness of internal combustion engines. The piston ring-liner assembly has three main purposes; seal the combustion chamber, control the lubricating oil, and transfer heat from the piston to the liner. Despite its important functions, the piston rings and liners are also the source of the most frictional losses in an internal combustion engine. Research has demonstrated that frictional losses in piston assemblies can reach as high as 50% of total engine friction.

Analytical methods of exchange in piston ring lubricating were the first type of studies undertaken. One of the first of these studies was done by **Furuhama (1959),** which developed a transient model of Piston ring lubrication with a one-dimensional Reynolds equation. The primary objective of this study was to investigate the hydrodynamic oil film created between the piston ring and the cylinder liner with some measure of support from experimental data obtained from actual experimentation or field use.[4], [5]

In addition to their mechanical and thermal properties, the lubrication model of **Dowson** and **Ruddy** accounted for the physical properties of the film thickness, friction forces, and ring movement. This model enhanced the accuracy in predicting the relationship between the oil film on the ring and the liner contact point, along with the performance of the ring's lubrication function.

The subsequent developments considered the surface roughness in the lubrication theories. The **Average Reynolds Equation** with flow factors **by Patir and Cheng** enabled modeling for mixed lubrication conditions. In addition, a model by **Greenwood and Tripp** for predicting asperity interaction for rough surfaces was used for boundary friction in piston rings.

Gas flow and blow-by modeling in the piston ring pack

The gas flow models of the initial development based on the labyrinth seal configuration of a rig pack consisted of a gas flowing through the small volume of crevice fluids (defined as gas flow out of the cylinder and into the adjacent cylinder) between the piston rings and the cylinder walls. The gas dynamic model of gas flow developed by Eweis is widely used for estimating the amount of gas that can flow out of the crevice volume under the assumption of isentropic flow.

The later work of Namazian and Heywood involved the development of coupled models of gas ring motion where (1) blow-by and reverse blow-on-rings are mutually dependent and (2) how blow-by and reverse blow-by affect piston ring gas flow between the piston ring and cylinder wall. [6]

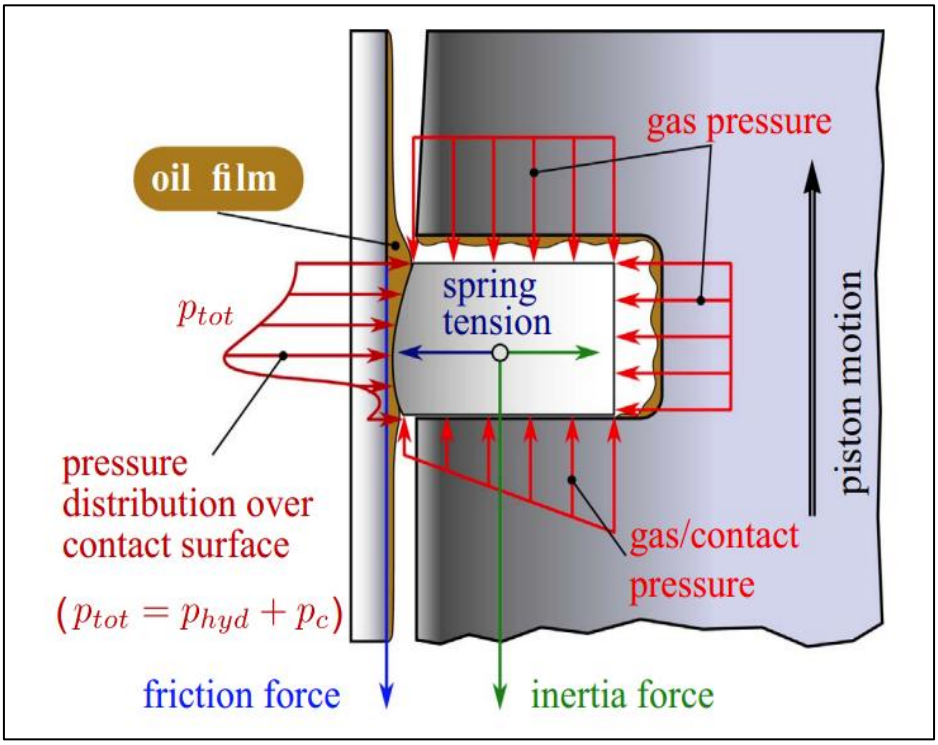


Figure 2.1 Balance of forces on piston ring.

2.2 Hydrogen-Fuelled Internal Combustion Engines

Hydrogen has gained considerable interest as a promising alternative fuel source for IC engines because of its potential to minimize the emission of carbon.

Hydrogen combustion is quite different from other hydrocarbon-based fuels because of the following characteristics:

- Higher flame propagation speeds
- Lower ignition energies
- Lower density

Hydrogen engines can also be subjected to a higher amount of blow-by due to a rapid rise in pressure during combustion and a lower density of hydrogen gas. This can result in a higher amount of gas passing through the crankcase, making it necessary to install ventilation systems in these engines.

Another major issue associated with hydrogen-fueled internal combustion engines is related to their tribology. Hydrogen can cause degradation in lubricants used in these engines, along with a higher amount of wear in piston ring contacts due to a higher temperature produced during combustion.

2.3 Friction and Energy Loss Studies in Alternative Fuel Engines:

Recent studies have also investigated the impact of alternative fuels such as hydrogen and compressed natural gas on piston ring friction.

Research on hydrogen and CNG engine comparisons found that hydrogen engine friction may be higher due to increased combustion pressure.

The choice of materials for piston rings is also of critical importance for friction reduction and ring life extension. Various materials have been investigated:

Cast iron, High-strength steel, Silicon nitride.

Silicon nitride rings were found to be beneficial in high-pressure hydrogen engine environments.

Chapter 3: Methodology

3.1 Two-dimensional (2D) CFD Model of the Piston Assembly

Since 3D CFD models are still very calculation-intensive, a 2D CFD model has been developed, which considers many system characteristics of the system under consideration, the piston assembly in a diesel engine. The calculation of the oil and gas phase flow through the ring pack is coupled with the piston ring dynamics. The piston ring dynamics are described using a classic motion equation according to Euler. The ring twist is determined using a simple approach, considering the moment equilibrium and the torsion stiffness of the ring. The pressures in the interfaces between the piston ring/liner and ring/groove, due to solid contacts, are considered using an integral solid contact pressure curve, which is calculated using a discrete solid contact model. The calculation of the fluid flow into the clearances between the rings, piston grooves, and liner, as well as into the entire flow field, is performed using the CFD. The flow through the ring end gaps cannot be considered directly in the 2D model and, therefore, is described using a labyrinth model.

The relative motion between the components like the piston and the piston ring could be considered in CFD modelling only through dynamic meshing. With the changing geometry of the computational domain due to the relative motion of the piston and ring, the mesh would also have to change its configuration accordingly to conform to the new domain geometry. While the complete dynamic mesh feature was not available for implementation in ANSYS Fluent, an innovative method for controlling the motion of the dynamic mesh was devised and implemented within the CFD model using UDF coding. The novel method involved displacing each node of the mesh independently according to the deformation caused by stretching and compression due to the relative motion of the boundaries of the piston ring and piston groove walls.

Summary of model used in piston ring dynamics studies:[7]

Physical Mechanism	**Mathematical / Analytical Model Applied**
Gas forces generated due to blow-by and blow-back flow	Orifice volume-based flow model
Lubrication force acting between the piston ring and cylinder liner	One-dimensional Reynolds equation considering mixed lubrication conditions
Contact force occurring when the lubricant film becomes insufficient	Greenwood–Tripp asperity contact model
Dynamic motion of the piston ring	Newton's translational equations and Euler's rotational equations of motion

3.2 Piston ring leakage model and used control equations:

The piston ring provides four pathways for gas to leak from the combustion chamber of a cylinder. These four pathways are illustrated in Fig.3.2; they are defined as follows:

First, the gas can escape from the piston ring as indicated by the blue arrow.

Second, the gas can escape from the gap between the piston ring as indicated by the red arrow.

Finally, the gas can escape from the piston ring to the groove of the piston ring as indicated by the green arrow.[8]

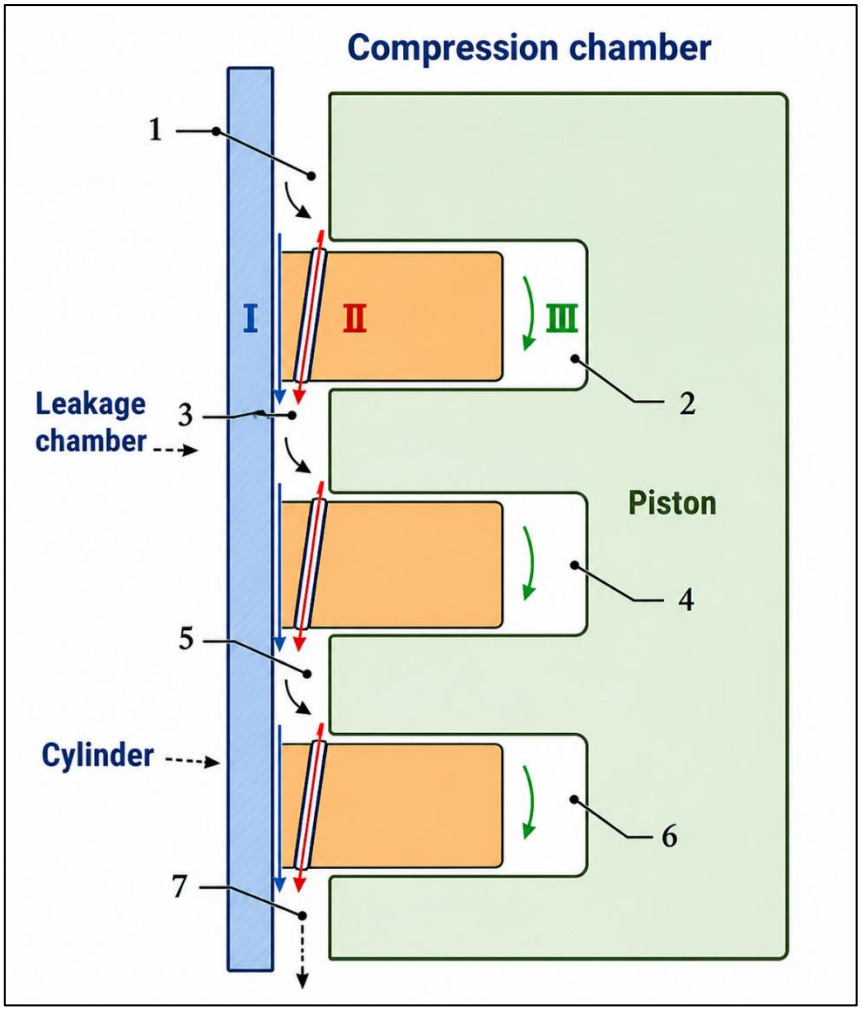


Figure 3.1 Leakage diagram of piston ring

3.3 Gas leakage equation:

Orifice throttling equation: The leakage through the cut of the piston ring can be regarded as a one-dimensional compressible adiabatic flow. It can be assumed that

Since the pressure difference between the adjacent leakage chambers may be too large, the gas flow through the cut can be divided

into subsonic and sonic flow. Gas leakage through the cut can be expressed as follows:[8]

$$\begin{cases} \dot{m}_{cut} = \dfrac{dm_{cut}}{dt} = C_{cut}A_{cut}p_{up}\left(\dfrac{2}{ZR_gT_{up}}\right)^{\frac{1}{2}}\left\{\dfrac{\kappa}{\kappa-1}\left[\left(\dfrac{p_{dn}}{p_{up}}\right)^{\frac{2}{\kappa}} - \left(\dfrac{p_{dn}}{p_{up}}\right)^{\frac{\kappa+1}{\kappa-1}}\right]\right\}^{\frac{1}{2}}, \dfrac{p_{dn}}{p_{up}} > \left(\dfrac{2}{\kappa+1}\right)^{\frac{\kappa}{\kappa-1}} \\ \dot{m}_{cut} = \dfrac{dm_{cut}}{dt} = C_{cut}A_{cut}p_{up}\left(\dfrac{2}{ZR_gT_{up}}\right)^{\frac{1}{2}}\left[\left(\dfrac{2}{\kappa+1}\right)^{\frac{\kappa+1}{\kappa-1}}\right]^{\frac{1}{2}}, \dfrac{p_{dn}}{p_{up}} \leq \left(\dfrac{2}{\kappa+1}\right)^{\frac{\kappa}{\kappa-1}} \end{cases}$$

Where; C_{cut} is a coefficient that is related to the flow of a gas passing through the cut of a piston ring.

A_{cut} represents the leakage area at the cut of a piston ring and can be calculated using the formula of the cut length multiplied by the gap between the cylinder and the piston.

Z represents the compression coefficient of the stationary control volume gas.

κ is the isentropic index of the gas.

The high and low-pressure values of the upstream and downstream leakage chambers are noted as pup and $p_{dn.}$ The temperature in the upstream leakage chamber of the piston ring is Tup.

The empirical formula is used to generate a flow coefficient. The flow coefficient is then modified by the ratio of upstream to downstream pressures.[8]

$$C_{cut} = 0.85 - 0.25\left(\frac{p_{dn}}{p_{up}}\right)^2$$

Asperity Contact Model: A model of contact which considers the actual surface topographies is required to determine the friction losses caused by both the viscosity of the thin lubricant film and the friction between two rough surfaces. The Greenwood & Tripp model will be used for determining the load ratio between a body and its surface due to the asperities. This model assumes that heights of the

summit have a Gaussian distribution; thus, the relations between forces and compliances will be based upon statistical distributions of points on the surface.

Heat transfer equation: Heat transfer between the control volume and its surroundings at any instant of time may be represented as follows:

- $\dot{Q}_{\text{heat}} = \frac{dQ}{dt} = h_{\text{heat}} A_{\text{heat}} (T_c - T_{\text{wall}})$

where h_{heat} denotes the convective heat transfer coefficient and A_{heat} represents the heat transfer area. The term T_{wall} corresponds to the wall temperature of the control volume.

The heat transfer coefficient is defined as follows:

- $\mathrm{h}_{\text{heat}} = 3 \cdot 0.7 \cdot \frac{\lambda_c}{D} \left(\frac{\rho_c U_{\text{mean}} D}{\mu_c} \right)^{0.7}$

In the heat transfer formulation, $\lambda_c$and $\mu_c$denote the thermal conductivity and dynamic viscosity of the working gas, respectively. The parameter D represents the cylinder diameter, while U_{mean} refers to the average piston speed.

3.4 Piston ring wear model:

Archard wear theory: Piston ring-cylinder liner wear is a complicated process which can be divided into three stages: the running-in stage, the stable wear stage, and the severe wear stage. Only the stable wear stage demonstrates a relatively consistent and predictable pattern of behaviour. Most of the research on wear and lifespan prediction for piston rings is based on the stable wear stage. Archard's wear theory is a classic method for the investigation of a wide range of tribological problems. Archard's theory defines the relationship between the volume of worn materials and various parameters, such as the hardness of the materials, load, and sliding distance.[8]

- $\mathbf{V_{WERAR}} = \frac{\boldsymbol{kwS}}{\boldsymbol{H}}$

Where V_{wear} refers to wear volume, W stands for the load, S for the sliding distance, H for hardness of soft material, and K for wear coefficient that is non-dimensional.

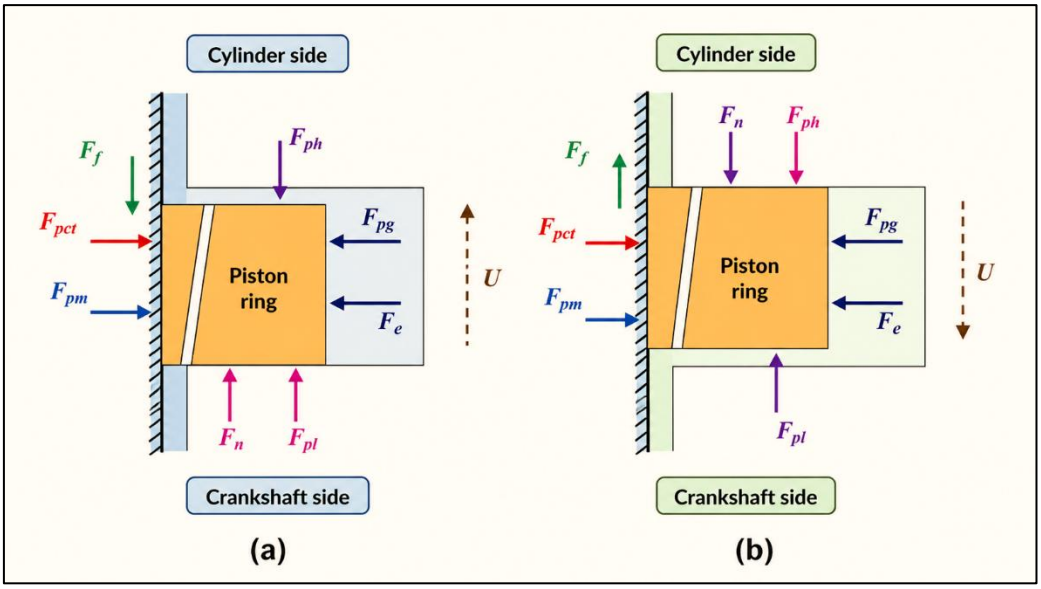


Figure 3.2 Force analysis with the piston ring positioned at the bottom (a) and at the top (b).

The primary function of the piston lies in its motion that affects the force acting upon the piston ring, and secondly, the piston's motion is related to its piston ring. The alignment of the piston and cylinder can be maintained for normal operation of the compressor by means of crosshead and rider bands. If the piston is correctly aligned and there is no contact between the piston ring's outer surface and the cylinder liner, then the secondary motion of the piston relative to the piston ring becomes nonexistent.[8]

However, in the reciprocation of the compressor piston, an instance might arise when the pressure exerted on the side facing the piston ring is smaller than that exerted on the rear end of the piston ring, hence the axial movement of the piston ring. When considering the forces exerted on the piston rings at their lowest point, the resulting equation is:

$$F_{ph} - F_n - F_{pl} + F_f = m_r a_r$$

$$F_{pg} + F_e - F_{pm} - F_{pct} = 0$$

The force exerted by the gas pressure acting on the piston face of the cylinder is termed as F_{ph}, while the force produced by the gas pressure acting on the crankshaft face is called F_{pl}.

F_n is the force produced because of the piston ring-groove interaction, while F_{pg} is the force produced because of the gas pressure acting on the groove of the piston ring. Fe is the force that is developed because of elastic deformation of the piston ring.

This force has a lower magnitude compared to the magnitude of Fpg; hence it can be considered insignificant since it has a smaller magnitude. This force acts radially and results from the average gas pressure in the space between the piston ring and the cylinder liner.

which may be given by-

$$F_{pm} = P_{up} + P_{dn}$$

3.5 Basics of CFD:

Continuity Equation:

$$\frac{\partial u}{\partial x} + \frac{\partial u}{\partial y} = \mathbf{0}$$

momentum conservation (Navier-Stokes equations):

The principle of momentum conservation is an important one within fluid dynamics, being concerned with the correlation between fluid flows and the forces exerted on them. This can be described mathematically through the Navier-Stokes equations, which are a set of nonlinear partial differential equations.

$$\rho\left(\frac{\partial \mathrm{V}}{\partial t} + \mathrm{V}\cdot\nabla\mathrm{V}\right) = -\nabla p + \mu\nabla^2\mathrm{V} + \rho g$$

And energy equation:

$$\frac{\partial}{\partial t}(\rho \mathrm{E}) + \nabla\cdot(\vec{v}(\rho \mathrm{E} + \mathrm{p})) = \nabla\cdot(\mathrm{k}\nabla T + (\bar{\bar{\tau}}\cdot\vec{v})) + S_h$$

And the stress tensor:

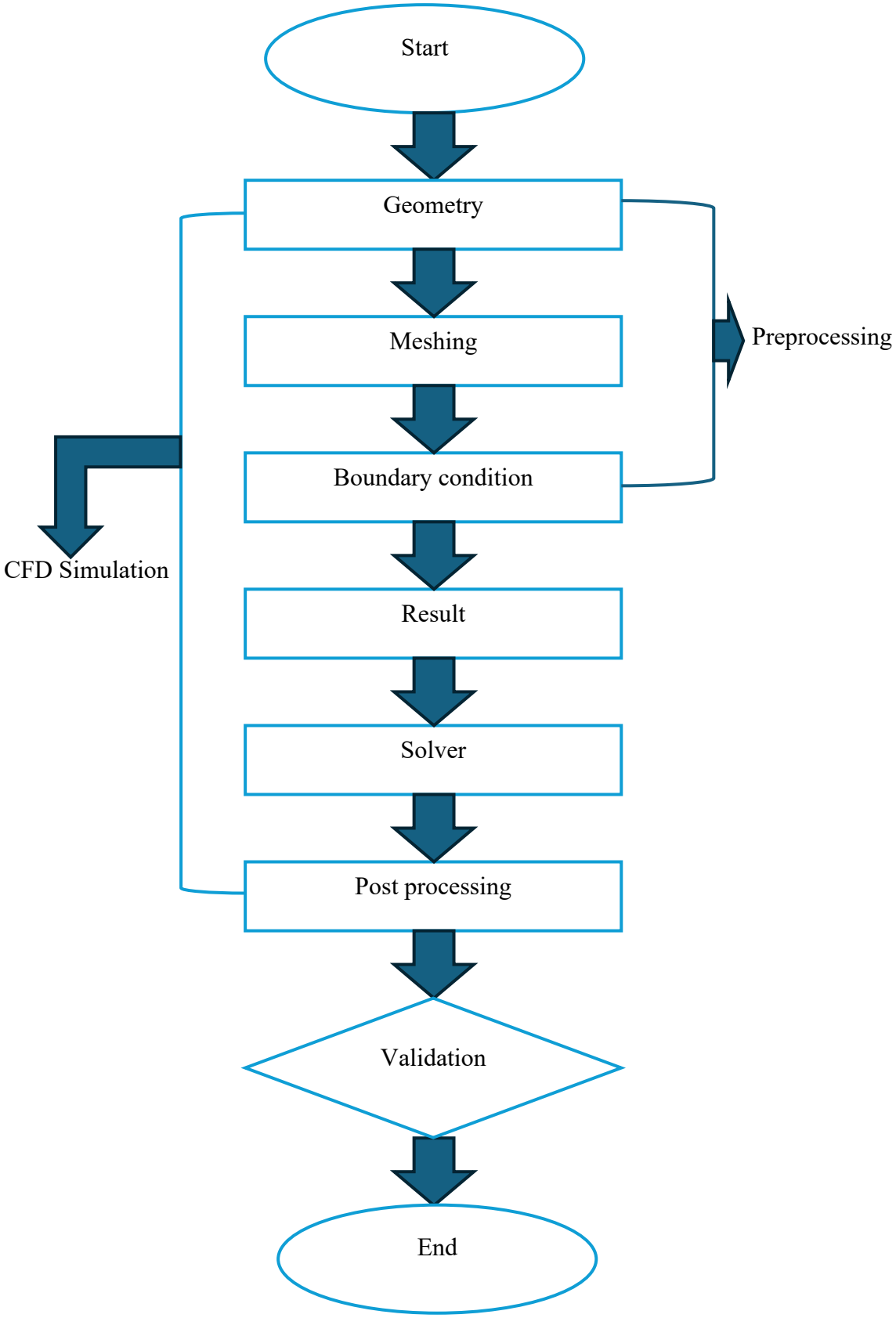
$$\bar{\bar{\tau}} = \eta \left[(\nabla \vec{v} + \nabla \vec{v}^T) - \frac{2}{3} \nabla \cdot \vec{v} I \right]$$

The exact vector form for the mass and energy transport processes formulated by Euler has an associated representation that can also be displayed by adding sources/sinks to the appropriate equations through use of the source terms S_m and S_h. Numeric discretization via CFD programs will generally be used to numerically solve these differential equations at the grid point locations specified by the digital representation of the fluid model using the Finite Volume Method (FVM).[9]

The formulation for the fluid flow equations, using the same representation method as above, consists of modifying the fluid flow equations to include the volumes associated with each individual phase, and the mass transfer of one phase to another through the evaporation or condensation of that particular phase (i.e. causing a phase change), or disruption (i.e. causing an implosion) by cavitation.

3.6 Simulation details:

Software employed: ANSYS Fluent (transient pressure-based solver). Geometry: Single-cylinder piston-ring-liner model. Ring-liner gap, ring-end gap, and ring-groove side gap are the leakage channels taken into consideration. The mesh used is a hybrid/structured mesh that is highly refined along leakage routes. The following dynamic mesh techniques were used: remeshing, layering, and smoothing. Displacement, depending on crank angle, describes piston motion. Flow physics: Hydrogen gas flow that is compressible. The energy equation for thermal phenomena has been solved. The ideal gas equation of state describes the characteristics of hydrogen. The pressure vs crank-angle function specifies the combustion chamber pressure. Constant reference pressure is used to specify crankcase pressure. The boundary condition is a no-slip wall. Two engine speeds were taken into consideration: 1500 and 4000 rpm. Crank-angle discretization is used to determine the time step.


Start
Geometry
Meshing
Boundary condition
Result
Solver
Post processing
Validation
End
Preprocessing
CFD Simulation

Discretization schemes for the second order were used. Criteria for convergence: residuals below 10^{-5}. The leaking outlet is used to monitor the blow-by mass flow rate. Over the course of one engine cycle, pressure and velocity fluctuations were examined. The piston head was subjected to transient thermal analysis. For displacement and stress, static structural analysis was done.

3.7 Model simplification and assumptions:

Uniform gas distribution: Gas within the compression and leakage chambers is homogeneous and has consistent thermal properties. Neglect deformation/failure - Effects of piston ring deformation from heating or fracture are ignored. Negligible chamber pressure effect - Gas leakage does not significantly influence compression chamber pressure. Fixed piston ring position -Axial movement of the piston ring is neglected; the ring is assumed to be seated at the groove bottom. Large groove clearance - Pressure in the ring-groove leakage chamber equals that in the adjacent leakage chamber. Kinetic energy dissipation- Leaked gas loses velocity; kinetic energy converts to thermal energy via collisions/friction. The values of suction and discharge pressures are considered constant, and the effect of valve action on suction and discharge operations is not considered. The values of suction and discharge pressures are considered constant. The effect of valve action on suction and discharge operations is not considered.

Upon reaching the leakage chamber through the piston ring, the speed of the gas becomes slow. The assumption taken here is that the energy of the gas in kinetic form becomes heat energy through collision and friction. Such an assumption makes the energy conservation equations simpler. The effect brought about by the lowering of the kinetic energy of the gas is neutralized.

3.8 Meshing Method:

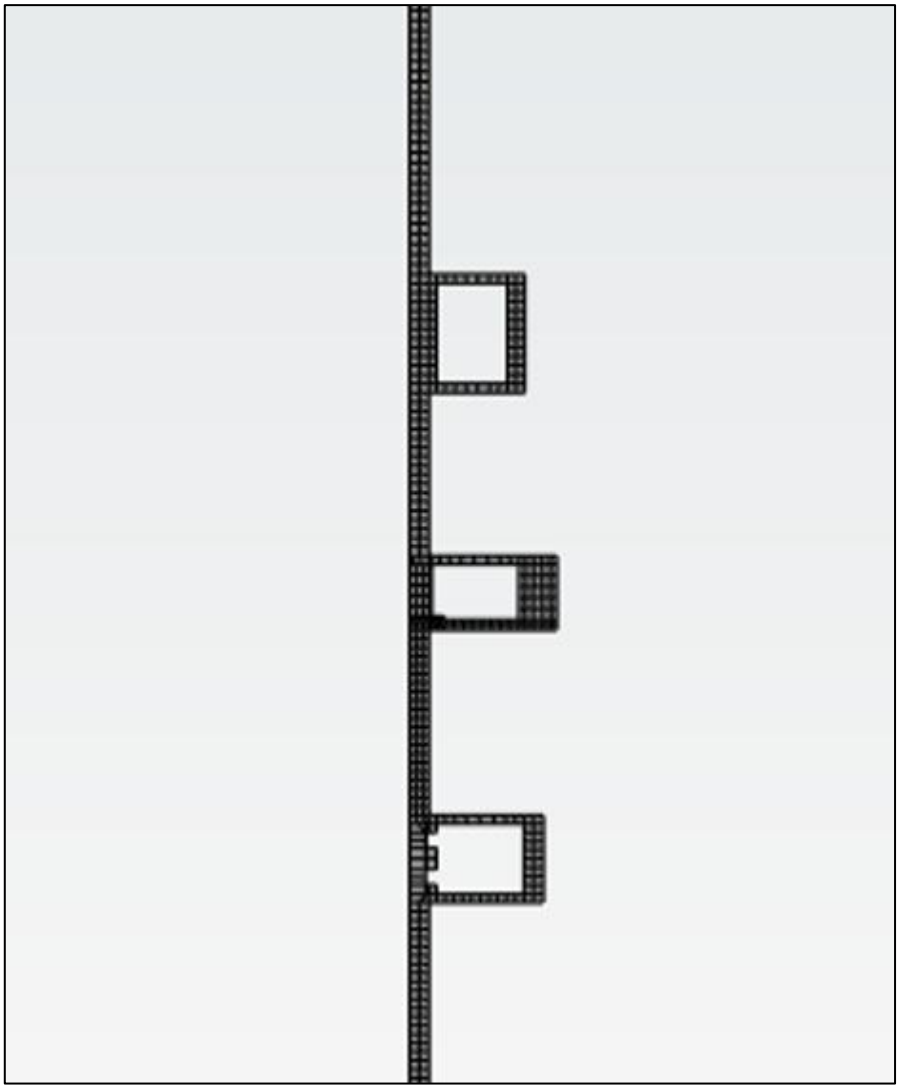


Figure 3.3 Manual Meshing of piston rings

CFD modelling was carried out on the 1.6 litre diesel engine taking into consideration detailed engine geometry and conditions. Geometry of the pistons was obtained based on the CAD drawing, and the geometry of the piston rings was defined based on the real cross-sections of the rings to consider the running face geometry. The design of the first compression ring was that of the keystone ring having a barrel-shaped running face, which is asymmetrical. Second compression ring was made of Napier ring having a taper shape while the oil control ring comprised bevel ring along with spring loaded coil and grounded land profile. Moreover, in addition to engine geometry modelling, the influence of thermal expansion and operation induced distortions in both piston and cylinder liner

geometries were also considered. The magnitude of deformation of the components due to these two factors was considerable since it was comparable to the clearances of piston-liner interface and piston rings-piston groove interface.

The ANSYS Fluent software package came into use for the CFD simulation. The computational mesh contains approx. 23,500 cells and was generated in the ICEM CFD program. The main objective of mesh generation for the CFD model was an achieving of a stable convergent transient solution for every time integration step. By the developing of the consistent mesh that on the one hand allows for the stable and accurate solution and on the other hand for the acceptable calculation time, it should be taken into account the problematic of the combination of macro geometry about 0.5–100 mm (interspaces between piston a liner, groove back space, combustor and crank case) and micro geometry about 0.3–80 μm (gaps on interfaces ring/liner, ring/groove flank and liner/skirt). The mesh size and mesh density distribution were adopted to fulfil these objectives. The fluid flow is described with the VOF (Volume of Fluid) multi-phase model with air as the primary phase, and oil as secondary phases. The estimated Reynolds numbers in the ring-pack crevices point to a laminar flow in these areas. Turbulences can occur in the combustion chamber, crank case and behind the rings. However, their influence on the entire system is disregarded in the actual model. A pressure-based solver with pressure/velocity coupling is used. A spatial 2nd order upwind discretization for momentum and energy conservation was selected to minimize discretization errors. Interpolation of the phase interfaces is done with the CICSAM discretization scheme, which is recommended for multi-phase flows with large viscosity ratios.[10]

3.9 Boundary conditions:

For the CFD calculations, the boundary conditions (BC) for a particular working point are shown under the conditions of 1500 rpm and IMEP = 4.3 bar (average combustion chamber pressure measured on an engine test bench) as a function of crank angle (based on theoretical combustion model) using gas pressure and crank angle to determine the average combustion chamber temperature using combustion process analysis to establish the appropriate average combustion

chamber temperature and using gas pressure crank angle as combust providing combustion pressures for CFD model, for; the combustion chamber pressure is supplied at the “pressure inlet”, as determined from the crank angle and supplied as an averaged pressure for use by CFD.

Using the same average temperature for establishing the BC’s; temperature would provide the foundation for establishing the combustion chamber temperatures using the “pressure inlet”, however; establishing the combustion pressure would be inadequate for establishing or setting the BC’s; temperature only for the “pressure inlet” provided the average combustive characteristics were obtained.

The fixed outlet pressure and temperature for both the piston liner and piston rings are 105N/m² and 354K, respectively. The fixed thermal boundary conditions (BCs) for the ring, liner, and piston are represented as a fixed temperature.

The oil properties for the 5W30 engine oil used in the CFD model are a function of temperature or pressure and are specified in the CFD model. The viscosity and density equations for the engine oil for temperature and pressure are provided. In the current CFD model, the shear thinning has been ignored because the used engine oil's temperature-dependent parameters (e.g. the high shear viscosity, the high shear critical shear rate and the high shear power-law index) have not been provided to use the Cross non-Newtonian model; however, incorporating shear thinning effects into the CFD model is generally recommended as it will improve the estimation of the radial gap height.[11], [12]

Parameter	Value	Unit
Cylinder diameter	135	mm
Piston diameter	132	mm
Liner	400	k
Ring 1	425	k
Ring 2	400	k
Ring 3	380	k
Groove 1	435	k
Groove 2	410	k
Groove 3	390	k
Piston crown	480	k
Piston bottom	370	k
Piston lands	400	k
Pressure inlet	4.3	bar
Pressure outlet	1.01325	atm

Figure 3.4 Required Boundary conditions parameters for thermal calculations

3.10 Dynamic Mesh:

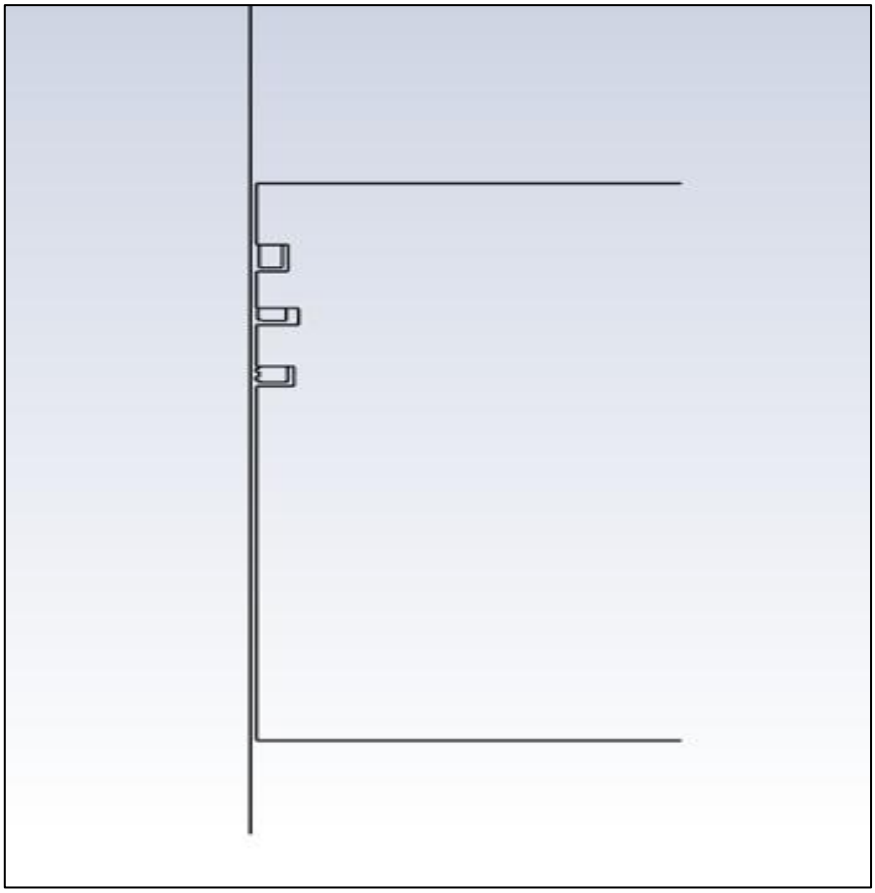


Figure 3.5 Dynamic Meshing

Smoothing: Adjusts the existing mesh node positions without changing mesh topology. Works like an elastic deformation: elements stretch or compress smoothly. Best for small boundary movements where cell shape remains acceptable.

Layering: Adds or removes layered cells near moving boundaries (e.g., piston face or ring groove). Works well with structured meshes and simple translational motion. Useful for sliding boundaries, valves, or piston linear motion.

Remeshing: Rebuilds mesh locally when it becomes overstretched or skewed. Allows adaptation to complex or large motions (ring movement, twisting, piston translation). Ensures mesh remains stable and prevents negative cell volume errors.

4.1 Steady State thermal analysis of Piston Ring:

4.1.1 Total deformation of piston ring

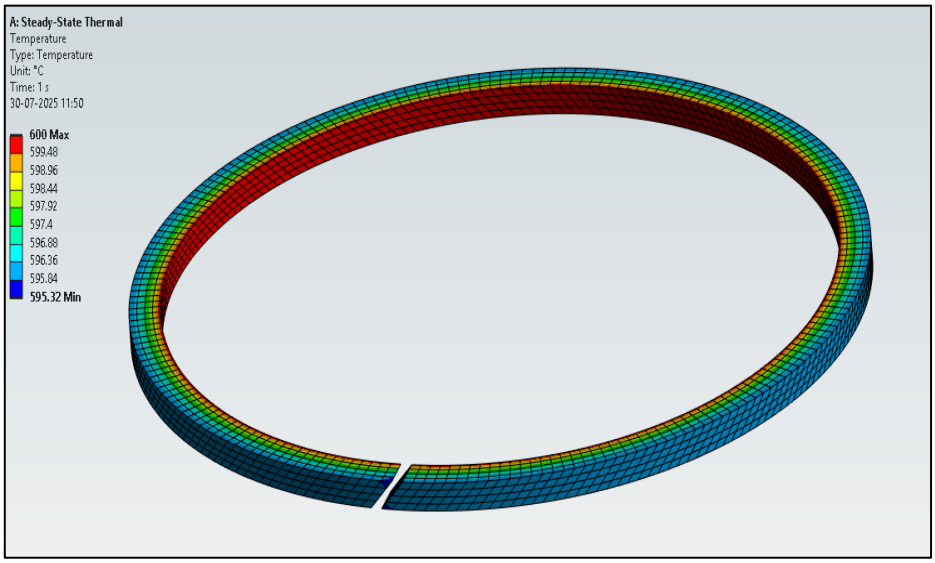


Figure 4.1 Total deformation of piston ring

This diagram displays the temperature distribution around the circumferential ring at steady state and once thermal equilibrium (no change in temperature with time) has been achieved. The temperature scale on the left shows a relatively small temperature range (between about 595.32 °C (minimum) and 600 °C (maximum)), giving a total temperature difference of only about 4.7 °C for the entire ring. The colour contour plot indicates that the inner surface of the ring has a greater thermal gradient (red area) than the outside surface (blue area) with a gradual transition between them. This indicates that heat is being transferred away from the inner circumference in a radial manner toward the outer circumference, showing the similarities between this behaviour found in an engine where the inside of a piston ring (where hot combustion gases are located) is much hotter than the cylinder liner (where heat is removed from the cylinder lining).

The grid structure found on the geometry shows that the grid is made up of structured quadrilateral elements. This suggests that a moderate degree of refinement has taken place in the overall mesh, thus enabling a reasonably accurate representation of the thermal gradient. The distribution around the entire

circumference of the ring is relatively uniform, thus indicating that axial symmetry exists for this thermal flow, except in the region immediately surrounding the small ring gap (representing the actual piston ring end gap), which causes a slight disruption in the thermal field in the vicinity of the gap and causes small variations within the thermal field.

4.1.2 Total Heat Flux of piston ring:

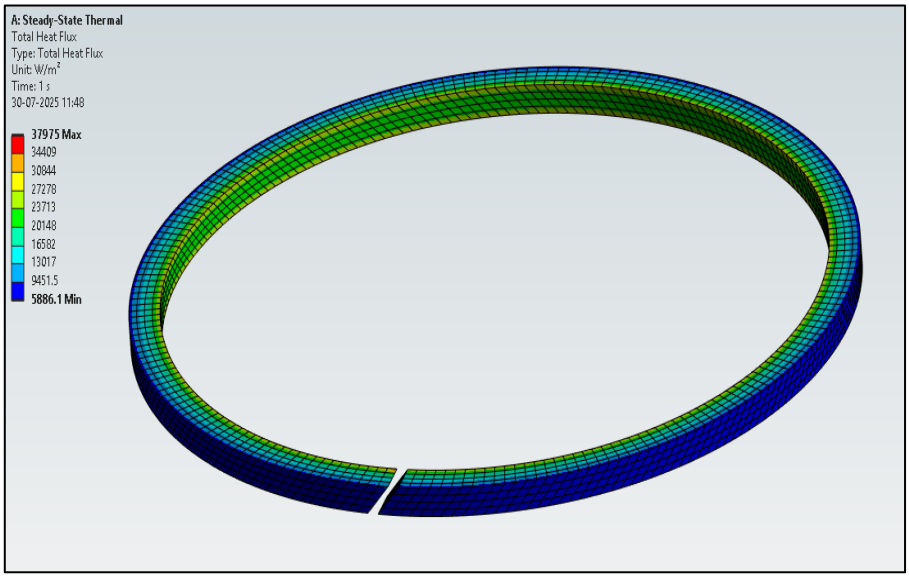


Figure 4.2 Total Heat Flux of piston ring

This image illustrates a thermal analysis of a circular ring piece (likely a piston ring) rendered in ANSYS (numerical thermal analysis software). The type of analysis depicted is a steady state thermal analysis that shows local heat flux (i.e. W/m^2) for the entire area of the ring (after steady-state thermal equilibrium has been achieved) demonstrating the total amount of thermal energy transfer per unit area. The heat flux is reported as having values ranging from a minimum of about 5886 W/m^2 (dark blue regions) to a maximum of approximately 37975 W/m^2 (red regions), which can be found throughout the entire thickness of the ring (displaying a large gradient across it).

The maximum heat flux occurs at the inner perimeter of the ring, while minimum heat flux occurs at the outer perimeter of the ring. Each ring's insulated boundaries and lateral conductive heat transfer show that the heat is generally moving radially outward from the inner portion of each ring to the outer portion of each ring.

The distribution is indicated in the plot of colour contours as red, yellow, and green bands appear close together and blue and cyan bands appear spaced further apart away from the centre of the ring toward the outside of the ring. This would be as expected if there was an elevated temperature working fluid (for example, combustion gases from an engine) acting in contact with the inner face of the ring and the outer face of the ring receiving cooling from the surrounding cylinder liner.

4.2 Static Structural analysis of Piston Head:

4.2.1 Total Deformation of piston head

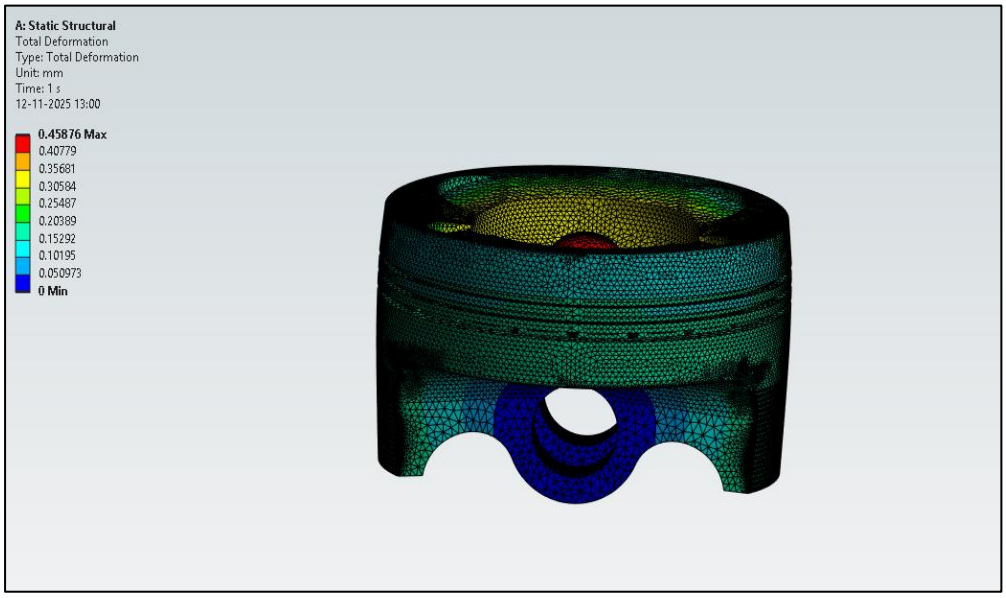


Figure 4.3 Total Deformation of piston head

This image shows an example of a steady-state thermal simulation result focused on a piston ring geometry and is thought to represent a very low magnitude field such as deformation, contact gap or another near zero-sized scalar value such as displacement or leakage related parameters; based on these numbers found on the legend that show values of 0 up to approximately 0.05 (with units being obscured, however are most likely to have been given in either mm or as a normalized value); . The piston rings were modelled with a fine structured hexahedral mesh composed of quadrilateral elements so that the resolution of gradients across the thickness and along the circumference was correct. The rest of the piston rings are predominantly shown in various shades of green, indicating a relatively even, low value in each of the ring sections; however, there is also a narrow concentration or peak located in one small

area in the top portion of the ring that shows a slightly higher value in this case yellow/red colours were used and indicate a higher concentration.

The general distribution is found to be essentially axisymmetrical, indicating that the physical behaviours of the ring are approximately the same everywhere around the entire diameter with few small variations being caused by boundary conditions, contact conditions or by geometric discontinuities like the gap in the ring itself. The fact that the minimum value is very close to zero suggests that there may be some areas of little or no deformation or clearance, which is typical during steady state conditions when a system is stable, as well as not subject to external forces.

4.2.2 Equivalent Elastic Strain of piston head:

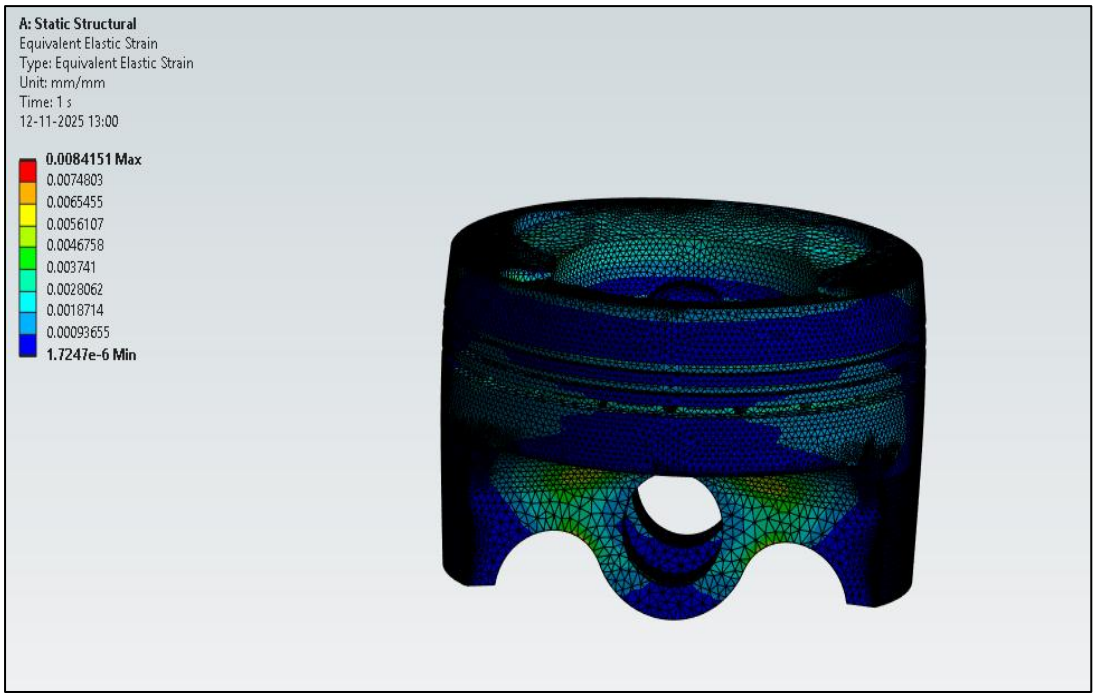


Figure 4.4 Equivalent Elastic Strain of piston head

This picture captures yet another steady-state simulation result showing the piston ring geometry and what appears to be some parameter with low magnitude values likely related to leakage flow, film thickness or micro-scale deformation/contact behaviour. As per the legend, these values range from a minimum of about 1.7247 x 10^{-6} to a maximum of around 0.0018 (the units are not visible on the picture, but they are most likely either metres, millimetres or some type of flow related parameter used in these types of studies) which suggests that the differences

measured across the ring are quite small and at the micro scale level. Most of the area represented by the contour plot (dark blue) appears to have low values for the parameter with slight increases (represented by the cyan/blue) primarily located near the upper surface and within specific regions of the ring, indicating that there are very few specific locations where the concentration of the parameter is greater. Additionally, the mesh (fine structured) used in the model provides a clear representation for all these small variations, with an adequately connected and only minorly distorted (compared to fully connected) mesh layout. The uniform (with respect to circumferential direction) distribution of the parameter indicates that the piston ring system is both stable and balanced when subjected to the current applied conditions; indicating there will not be any large asymmetries or distortions within this model. However, the minor amount of non-uniformity located at the very top of the piston ring may be due to localized thermal gradients (temperature), contact pressure (distribution of load) or some other aspect of the rings' behaviour.

4.2.3 Equivalent Von- mises Stress of piston head:

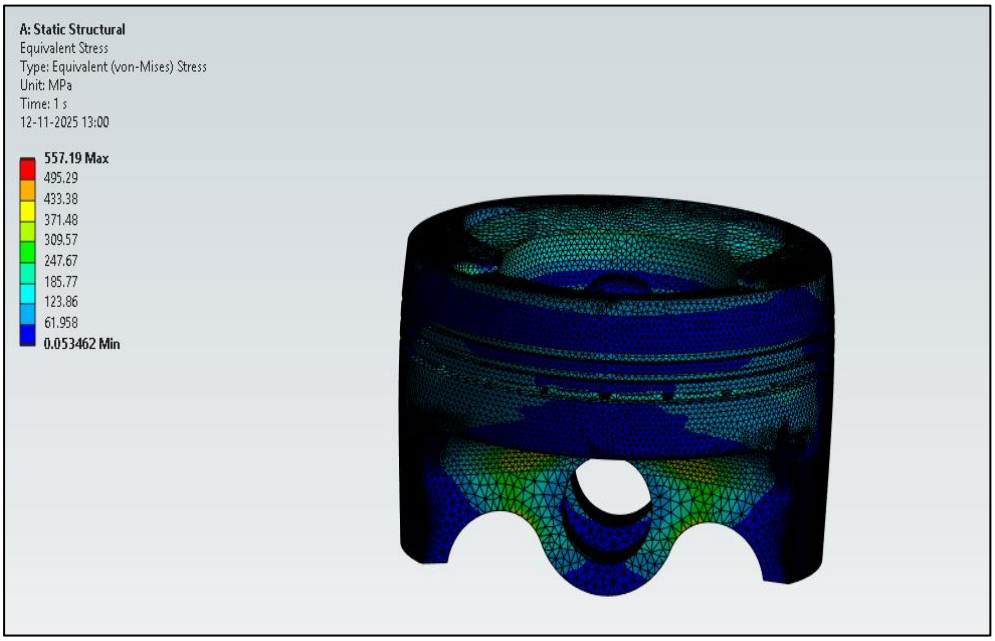


Figure 4.5 Equivalent Von- mises Stress of piston head

steady-state simulation of the piston ring, a plot has been created that displays one or more variables with their respective numerical values based on a given scale (for example, comparison of various pressure distributions can be shown using a colour

gradient). On the colour gradient provided with the legend shows that the values fall within the range of approximately 0.053 to about 123.86 Mega Pascals or Watts per square meter) will show that most of the surfaces of the rings are represented by the darkest blues, where lower value regions exist, and that there are some small regions in the rings along the top circumferential of the ring, which will provide some green and cyan tones suggesting that the parameter is not distributed evenly across the piston rings. The geometry for the piston ring is represented by a circular piston ring that has a gap in the middle and is meshed using a fine structured mesh. This structured mesh allows the modeller to accurately capture the gradients between the ring thicknesses and on the circumferences of the piston ring. There is also a predominant axisymmetric nature to the overall distribution of the rings, which indicates that the loading or boundary conditions applied to the rings are symmetrical about the longitudinal sections of the piston rings. However, there are some areas of slight variations from the symmetry, such as the top of the piston ring (possibly within the gap). These variations may be due to the contact with the liner of the cylinder, thermal gradients at the contact point or pressure of the combustion gas.

4.2.4 Safety Factor of piston head:

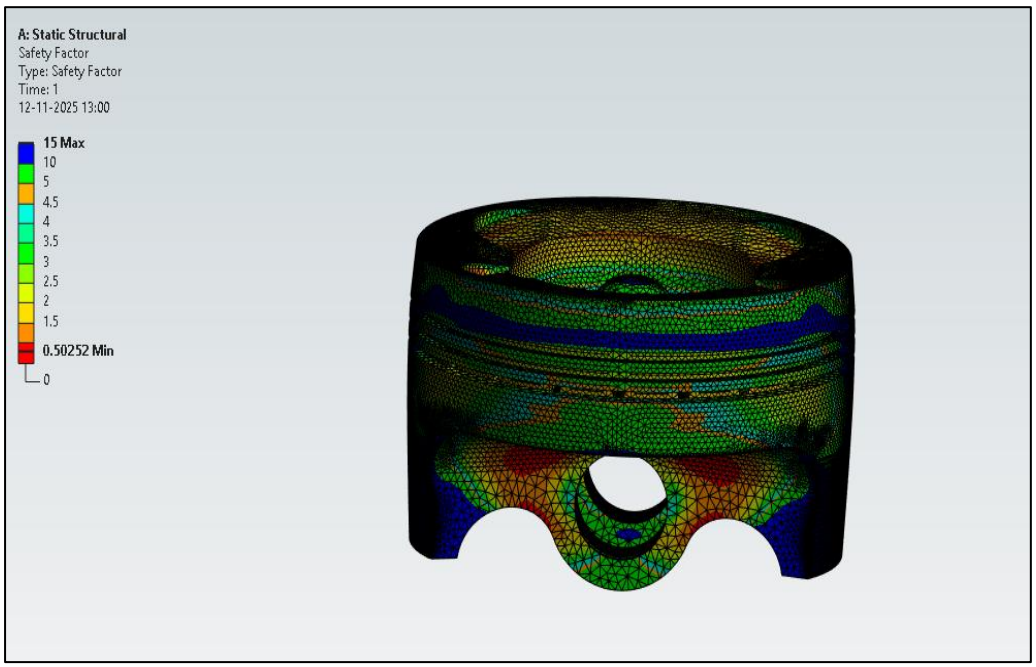


Figure 4.6 Safety Factor of piston head

The FEA image of the piston model shows static structural FEA results for the piston, color-coded with safety factors. The contour plot depicts safety factor distributions based on load applied to the piston, ranging from approximately 0.50 (minimum) to 15 (maximum). The colour scale is based on a gradient from red (failure/critical regions with low safety factor) to yellow and green (moderate safety) to blue (safe; over-designed with high safety factors).

The most critical areas of the piston are found respectively at the piston skirt cut-out and pin boss, with the cut-out showing much higher concentrations of high-stressed areas (red/orange) and low safety factors relative to the design limits of safety. With respect to the critical region, dull green/yellow indicate moderate safety design; therefore, adequate, but under significant stress.

For the outer skirt (blue green), they show the highest degree of safety and may have overdesigned or through increase in material. The mesh used in developing the discretized finite elements has a fine triangular shape; therefore, can provide the necessary accuracy required to represent stress distribution through complex geometry. While most areas of the piston show adequate structural safety, there exists a need for possible redesign and/or material reinforcement in the pin boss and lower skirt areas.

4.2.5 Life of Piston head of piston head:

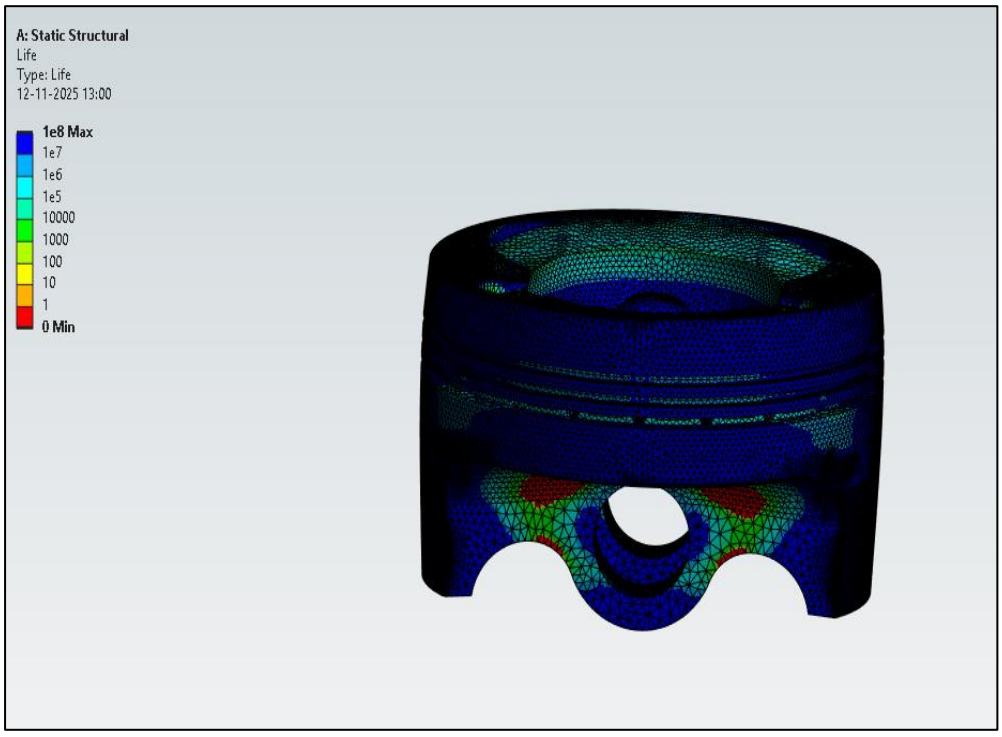


Figure 4.7 Life of Piston head of piston head

This is a report stating the prediction of how many cycles a component can take under cyclical loading conditions, find out by an analysis FEA (Finite Element Analysis) with regards to static structure. The life of the component (the number of cycles it can withstand prior to failure) ranges from 0 (minimum) cycles to approximately $1x10^8$ (maximum). The colour scale shows red indicating low life and blue indicating the highest life, i.e., critical failure zones (red) to safe/more durable zones (blue). The critical areas are clearly concentrated along the piston pin boss area and the lower skirt cut-out area. The colour scheme indicates these areas are at significant risk for crack initiation and/or catastrophic failure during operation (red and orange zones are low fatigue due to high cyclic stress concentrations). The remaining piston body (i.e., skirt and upper crown regions) illustrate the regions of very high fatigue life (i.e., the regions are structurally sound over the life of repeated loading) with blue to cyan colours. Mid-Skirt and ring land areas, which demonstrate moderate fatigue resistance (green to yellow), indicate that these areas have some cyclic stresses but will continue to perform normally. A fine triangular mesh was used for the analysis, thus providing a good prediction of the stress life at all the areas of the complex geometry. To conclude, while most of the piston appears to have a long fatigue life.

4.2.6 Damage of Piston head:

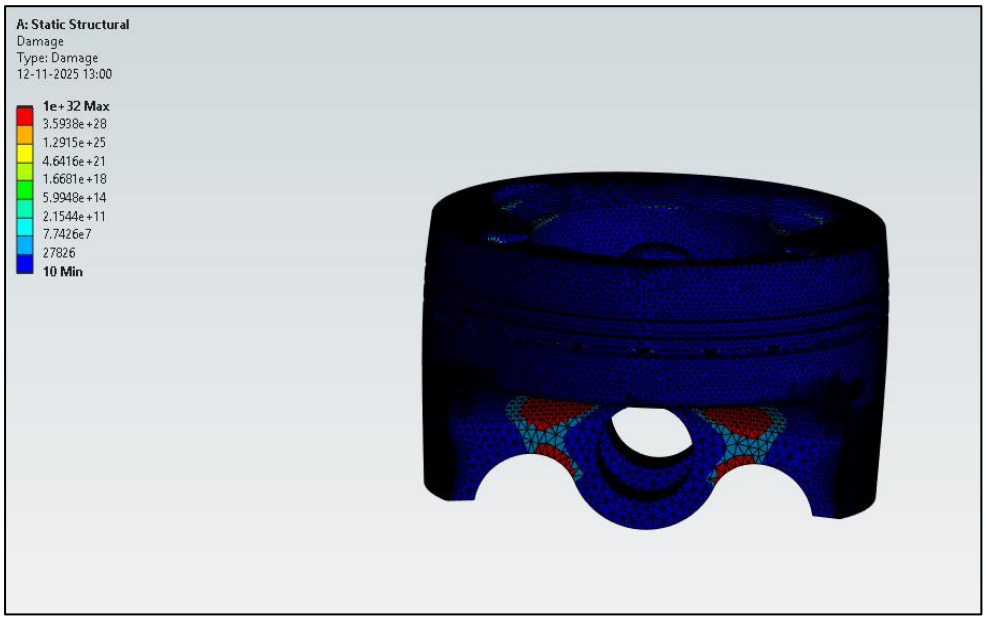


Figure 4.8 Damage of Piston head

The static structural damage analysis of a piston model displays the accumulated damage distribution associated with the applied load conditions. A damage scale has been applied to this analysis where 0 represents no damage and (10^{32}) represents a very large amount of accumulated damage (for example). Blue indicates areas with no accumulation of damage while red indicates areas that are close to failure. As seen in the image, most of the piston including the crown, ring lands and upper skirt are shown in dark blue colour, indicating minimal damage sustained by these components and therefore are structurally safe. The most obvious areas of high accumulated damage are around the piston pin boss and lower skirt cutout areas, where red and orange colour coding indicates areas with severe accumulation of damage due to the high concentration of forces and the cycling effect of loading. These are also the most likely points for initiation and propagation of cracks therefore the greatest risk for structural failure exists here. The areas of green, and light blue, at the transition of the critical areas are moderate accumulations of damage indicating a gradual distribution of stress from the critical areas. The use of fine triangular mesh improves the accuracy of capturing the gradients of damage, which is especially important in the areas where there are geometric discontinuities. Overall, the analysis suggests that all areas of the piston would be safe under the applied loading conditions, however, the pin boss and the lower skirt cutout would

be the most critical points to evaluate for future structural integrity.

4.2.7 Steady-State Thermal analysis of piston head

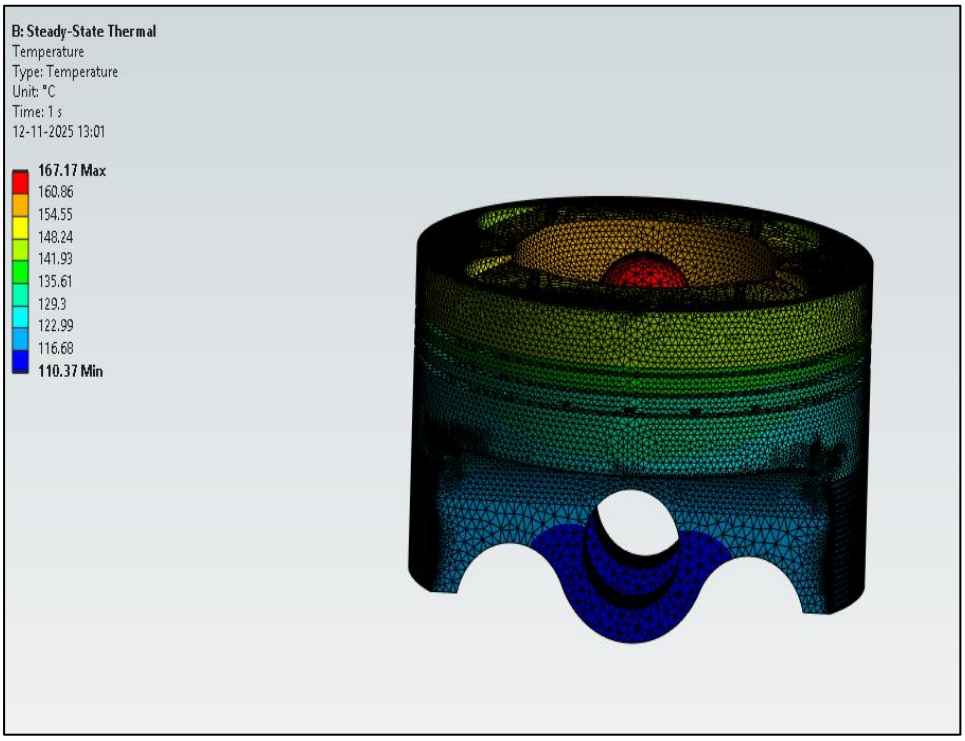


Figure 4.9 Steady-State Thermal analysis of piston head

The thermal distribution of the piston after equilibrium has been achieved is shown in this pictorial representation. The coldest point on the piston is approximately 110.37 °C (shown in blue) and the hottest point on the piston is approximately 167.17 °C (shown in red). A large percentage of the hottest temperature occurs at the crown (particularly in the middle) because of the continued exposure to the combustion gases (shown in red and orange). As you travel down the piston, the temperature becomes cooler, going through the ring lands and upper skirt (shown in yellow and green) due to the conduction of heat from the crown of the piston. The lower skirt and piston pin boss regions are predominantly blue to cyan since they have been cooled by oil (lubrication) and therefore are much cooler compared to other regions. The temperature gradient across the piston is more gradual than what was observed in transient testing and therefore indicates a more uniform thermal field. The small triangular meshes provide accurate representation of thermal gradients over complex geometrical shapes (on the surfaces of the piston). This analysis provides a representation of a realistic steady thermal profile of the

piston. The crown of the piston was consistently the hottest area of the piston and heat dissipated away from it toward the skirt of the piston, which is critical for predicting thermal stresses, material selection and long-term durability of the piston.

4.3 Transient thermal analysis of piston head:

4.3.1 Transient temperature analysis of piston head:

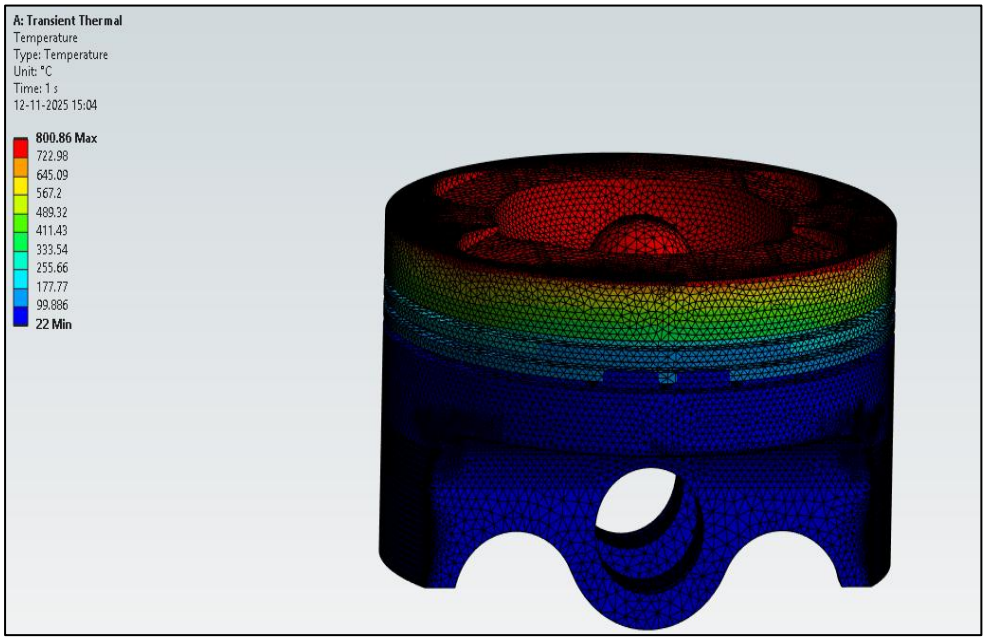


Figure 4.10 Transient thermal analysis of piston head

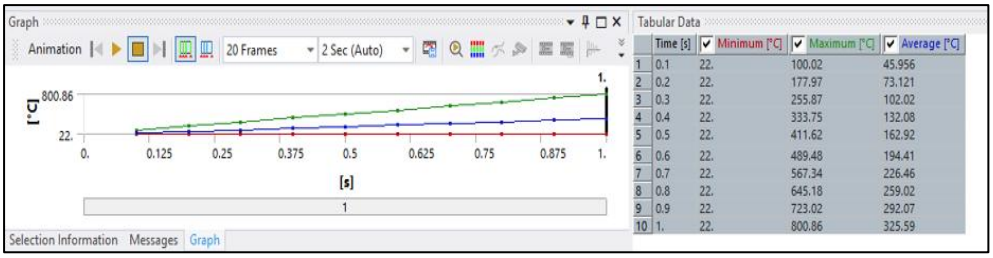


Figure 4.10.1 Transient thermal analysis tabular data

This is an image showing the transient thermal analysis of the piston for one second of time, with the temperature distribution through the part at that time. The temperature range has a minimum temperature of about 22 °C (blue area), and a maximum temperature of about 800.86 °C (red area) where there is a large thermal gradient throughout the piston as it operates. The area of the piston that has the highest temperatures is the piston crown (top surface), as it is in direct contact with

the hottest combustion gases, so it is shown in red/orange. As you move downward, the temperature continues to decrease gradually in the ring lands and upper skirt areas, as indicated by the yellow and green zones, through conduction of heat from the crown to the cooler regions. The lower skirt and pin boss areas are primarily blue, which shows that they are at much lower temperatures because they are relatively insulated from any combustion heat, and the temperatures in these areas are normally maintained with lubrication oil and surrounding air.

The relatively smooth thermal gradient from top to bottom demonstrates a realistic heat flow pattern, where conduction is the primary mode of heat transfer. A fine triangular mesh of the piston will provide appropriate resolution of the thermal gradients, especially along geometric discontinuities (ex., pin boss and skirt cutouts). This analysis demonstrates a high thermal gradient which is very important because the large temperature difference will induce thermal stress.

4.3.2 Transient thermal analysis at cross- section:

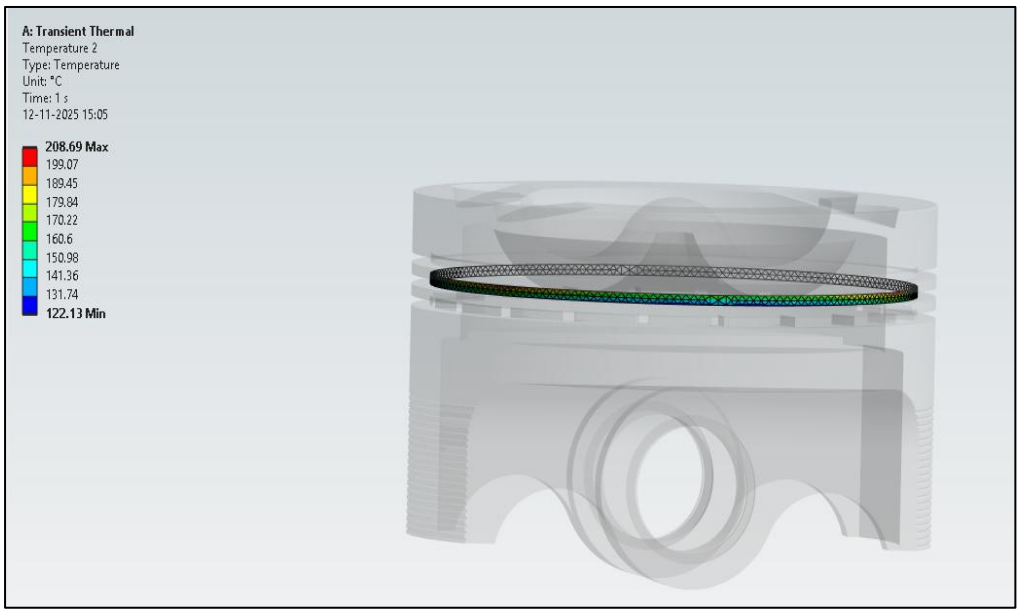


Figure 4.11 Transient thermal analysis at cross- section

This image represents transient heat flow of a piston from its top surface (Temperature 2) across a specific thin layer (cross-section) of about 1 second of the present time. The smallest temperature value is about 122.13 °C and the largest is about 208.69 °C. On this thin layer, which appears to be the crown thickness or ring land thickness, higher temperature values (yellow to light green) occur near the

outer edges, while lower temperature values (blue to cyan) occur near the inner edge. This is an indication that there is heat flowing outwards from the crown surface of the piston and then radially through the cooler part of the piston itself as well as the adjacent cooling structures. The semi-transparent piston model (back) illustrates the geometric configuration and the location of the thin layer (close to the crown of the engine), which also is consistent with the understanding that heat gradient across the thin section is due to both radial and circumferential heat transfer influenced by geometry, material properties, and boundary conditions (i.e., convection/conduction). The fine mesh provides good resolution of thermal gradients along the thin layer. The results of this study illustrate temperature differences in a critical area of the piston and are beneficial for understanding.

4.3.3 Transient thermal analysis of Total heat Flux:

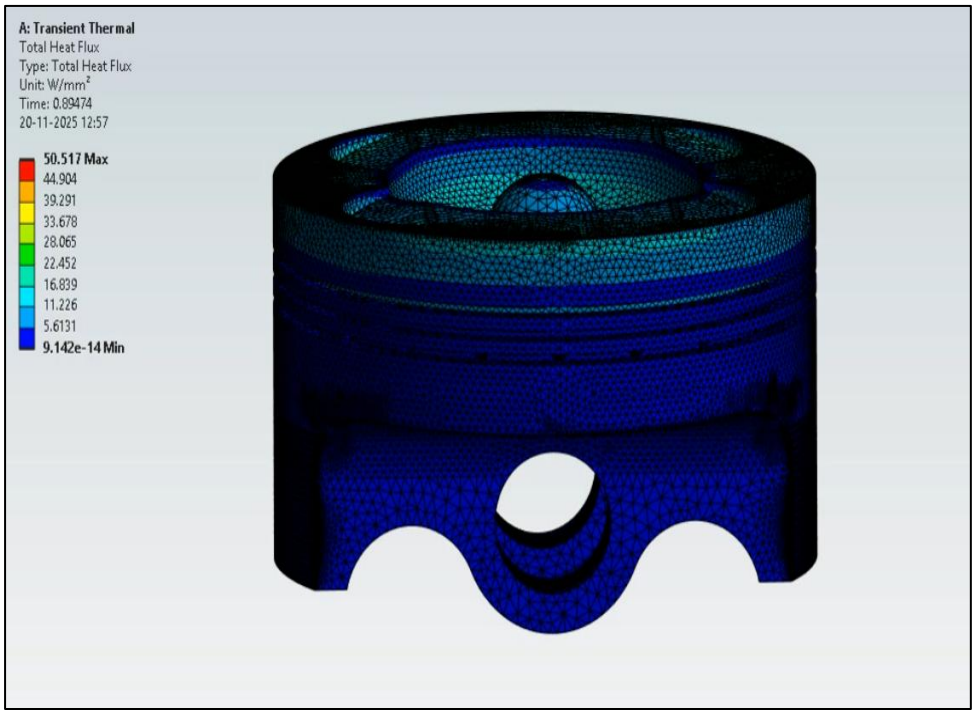


Figure 4.12 Transient thermal analysis of Total heat Flux

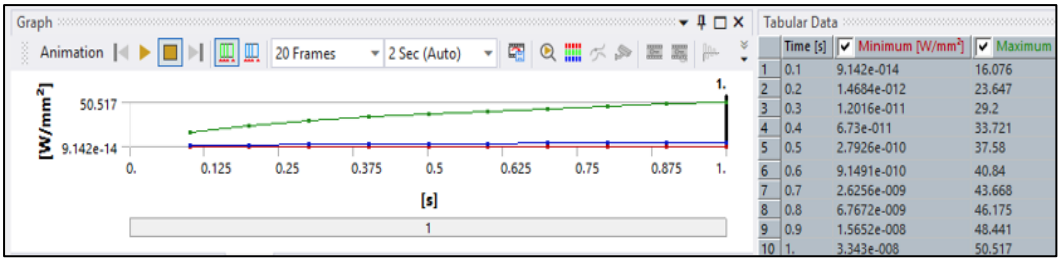


Figure 4.12.1 Transient heat flux analysis tabular data

A pictorial representation of the transient thermal analysis done on the piston identifies that total heat flux distribution at a single time step (0.89474 seconds) is being illustrated via the dimensions of the heat flow/millimeter squared (W/mm^2) from the minimum and maximum heat flow points (being close to 9.14×10^{-14} W/mm^2) up to about 50.52 W/mm^2. The major concentration of the greatest amount of heat is located at the crown of the piston and in the combustion bowl area, as indicated with the light blue to cyan colourings on the contour; this reflects that high levels of thermal heat transfer are present due to being directly in contact with high-temperature gases. In addition, moderate levels of heat have been experienced in the upper ring land area of the piston due to conduction taking place away from the piston crown. On the other hand, the lower skirt and pin boss areas of the piston show the largest area of dark blue (representing little or no heat) and are, therefore, relatively insulated by the surrounding materials they are in contact with and have experienced little thermal loads. The smooth transitions from the top of each area of the piston are indicative of the path that the heat takes as it travels from the combustion bowl area and/or along the length of the piston and towards cooler areas of the piston (primarily through conduction). In conclusion, the piston crown is the heat entry area, and the lower skirt of the piston is the heat exit area.

4.4. Piston Velocity graph at 4000 rpm:

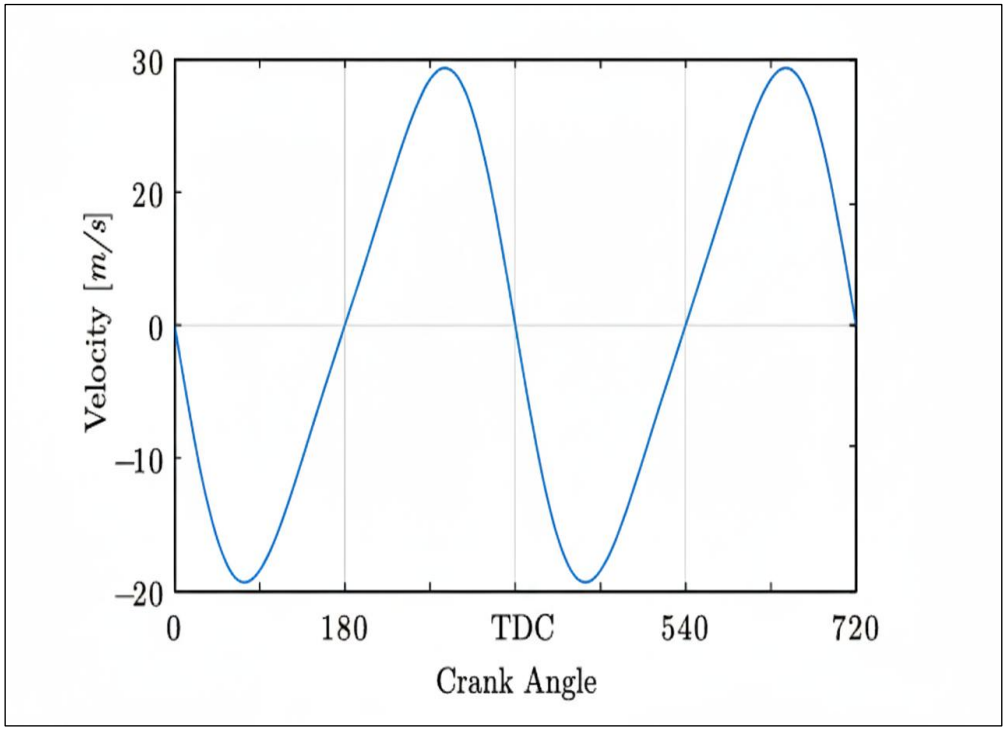


Figure 4.13 Piston velocity v/s Crank angle graph at 4000 rpm.

A graphical representation comparing the change in both piston speed (in m/sec) and the angle (in degrees) of the crankshaft from 0° to 720° represents two complete revolutions of the crankshaft in a four-stroke engine. The resulting speed profile of the pistons is sinusoidal, although slightly asymmetric due to connecting rod effects. Beginning at a dead centre dead centre (0°), the piston experiences a speed of 0 m/s and rapidly continues into a declining speed of approximately −19 to −20 m/s by approximately 90°. The speed continues to increase from a declining speed until the point where the piston reaches another dead centre at approximately 180°, so that there exists a change of direction of the piston's motion, followed by a maximum positive speed of approximately +29 to +30 m/s around 270° (maximum upward motion). The cycle repeats in a symmetrical manner during the second half of the cycle (360°–720°); again reaching a dead centre dead centre at around 360° resulting in speed equal to 0.00 m/s at these specified angles (0°, 180°, 360°, 540° and 720°) indicating that piston speed is equal to maximum magnitude between these specified dead centre/maximum speed changes (max [+ve] > max [-ve]), due primarily to the impact of crank rod angle relative to the crankshaft. Overall, from a graphical perspective, illustrates how the piston behaves dynamically.

4.4.1 Velocity contour for piston rings:

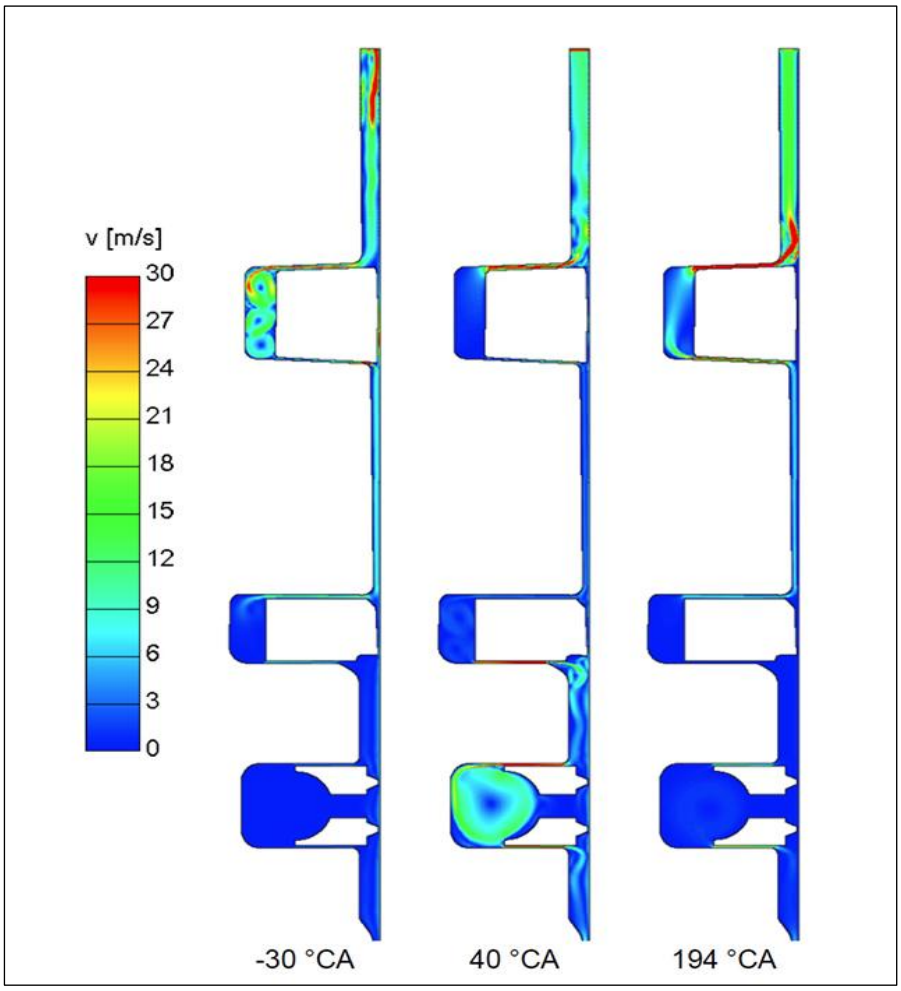


Figure 4.14 Simulations of Velocity contour for piston rings.

The picture illustrates a computational fluid dynamics analysis of the flow velocity distributed throughout the cylinder during three crank angle positions: −30° crank angle, +40° crank angle and +194° crank angle. The flow velocity is represented by a colour scale from 0 m/s (dark blue) to 30 m/s (red). At the -30° crank angle, which represents the intake phase, flow indicates a high degree of turbulence and swirling motion predominately near the intake port area with locally high (green and red) velocity regions depicting active inflow and mixing of air and low velocity (blue) regions indicating relatively stagnant flow. The +40° crank angle represents likely the compression phase; the flow at this crank angle demonstrates more gradual organisation, reduced intensity of turbulence, and has a more uniform distribution

of velocity than at the -30° crank angle while still having presence of moderate velocity ranges (cyan and green) close to geometric constraints outlined within the cylinder and near the piston bowl indicating continued motion and mixing of air. By +194° crank angle, the flow indicates distinct high velocity zones (red) near the exhaust valve and port exit indicating rapid discharge of exhaust gases. Most of the volume of the cylinder exhibits very low velocities (blue) at this crank angle indicating very little internal motion following combustion. The Figures show the major features of the engine geometry including intake and exhaust ports, and the piston bowl. Additionally, because of the crank angle variation the Figures illustrate the progression of fluid motion through the various phases of operation within an internal combustion engine.

4.4.2 Combustion pressure Graph at 1500 rpm:

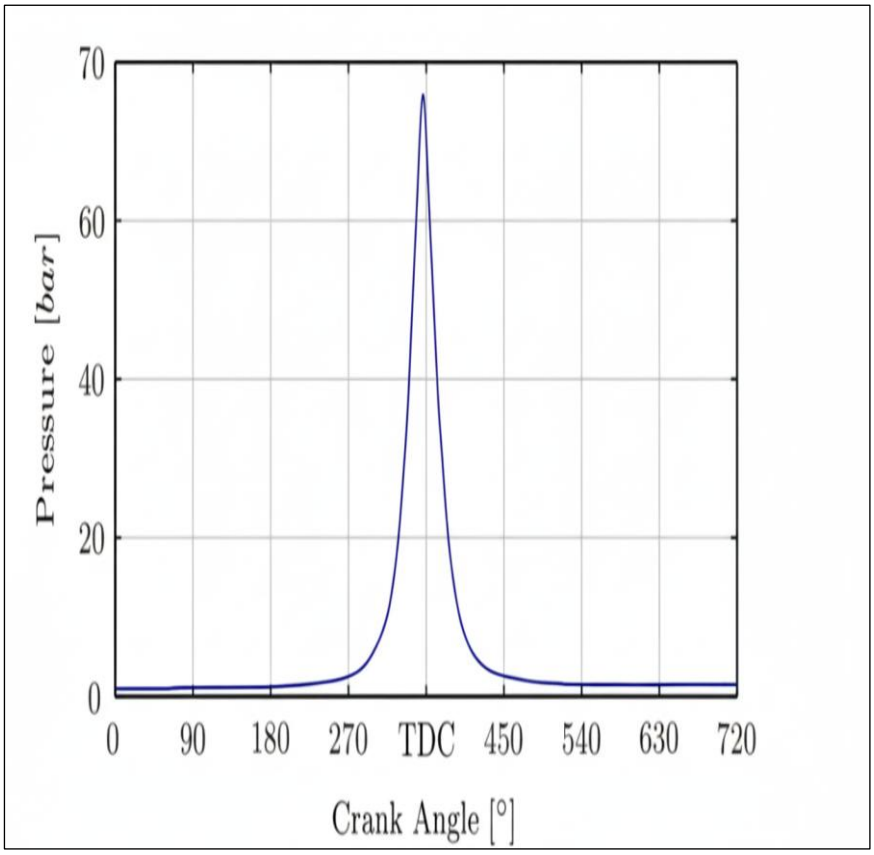


Figure 4.15 Combustion pressure at 1500 rpm

The graph shows the change in the in-cylinder pressure (in bar) against crank angle (in degrees) for a single revolution cycle in a four-stroke internal combustion

engine. The first stage starts with the intake stage where the pressure is very low, just above 1 or 2 bars, which can be attributed to the crank angle of zero degrees. Between the angles of zero and 180 degrees, the piston moves downwards, and the pressure level stays constant with only minor changes that are brought about by the movement of air-fuel mix inside the chamber. In the angles between 180 and 360 degrees, the pressure level gradually increases due to the compression stroke when the air-fuel mix is compressed in the cylinder by the movement of the piston upwards.

Just before TDC, there is seen an abrupt and extremely significant peak in pressure, peaking at a maximum pressure level of about 65-70 bar. This sharp increase in pressure indicates that combustion (or ignition) is taking place; the compressed air-fuel mixture ignites and burns, thereby producing a lot of energy within a very brief period of crank angle. The narrow and steep shape of this peak implies that there is practically no delay between compression and combustion, which shows an optimum level of efficiency. After achieving its highest point, as soon as the crank angle exceeds 360 degrees, the piston begins its descent motion, during which expansion takes place. The high-pressure gases expand, and work is done by them against the piston. The drop in pressure is sudden and steep initially but subsequently becomes slower.

In the range from 450° to 720°, during the exhaust and next intake stroke process, the pressure keeps falling again to reach another low value near the atmospheric pressure. As can be seen from the graph, it is relatively flat throughout this period because there are no combustion and compression in this phase. The graph shows all the thermodynamics of what occurs in the engine cylinder including intake, compression, combustion, and expansion phases where the low-pressure intake, the increase in pressure, combustion point (at TDC), and sudden decline are clearly observed in the graph.

4.4.3 Pressure contour for piston rings:

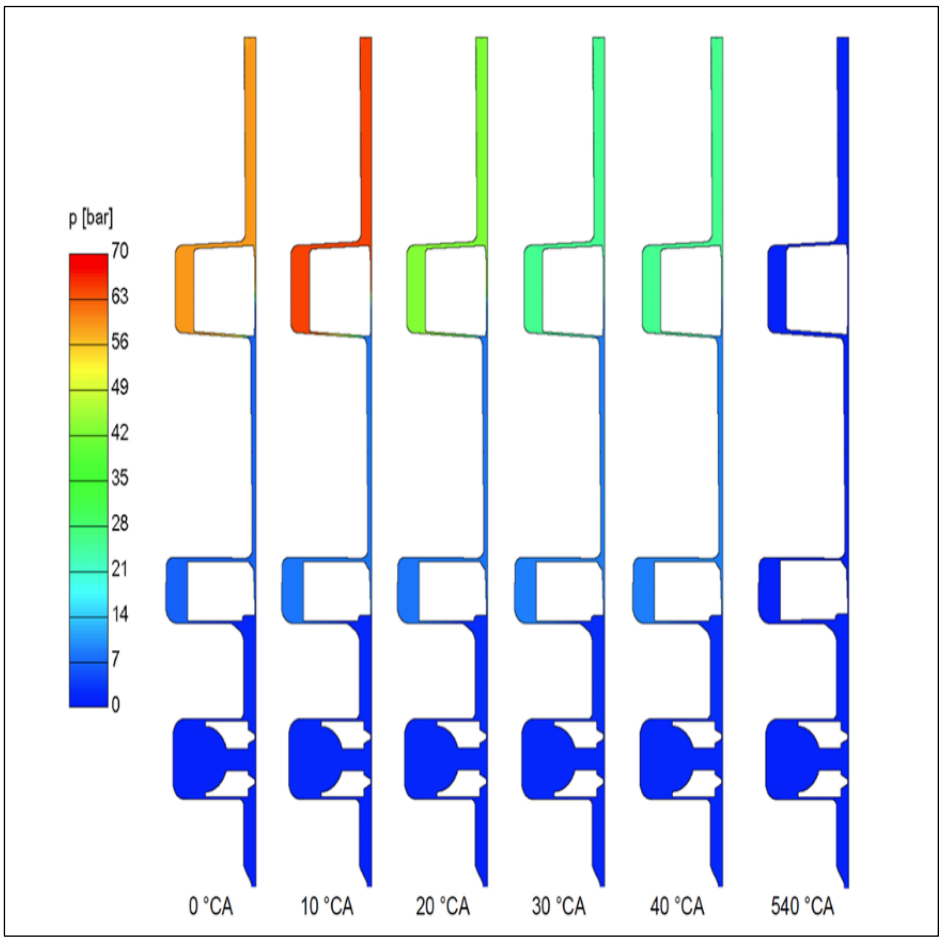


Figure 4.16 Pressure results at selected crank angles.

The plot shows a series of contour diagrams depicting the in-cylinder pressure distribution (bar) in an internal combustion engine at various crank angles (CA). The contour diagrams are presented for crank angles of 0°, 10°, 20°, 30°, 40°, and 540°. In the left side of the figure, a colour scale from 0 bar (dark blue) to approximately 70 bar (red) has been provided to identify the level of pressure in the combustion chamber and connected passages. For the crank angle of 0°, corresponding to the TDC, the pressure in the combustion chamber is maximum and reaches up to values around 65–70 bar (represented by red/orange colours). These values represent the highest-pressure levels that prevail near the piston crown in the upper cylinder due to the maximum energy release after ignition of the air-fuel mixture. At 10° and 20° crank angles, although there is a slight reduction in pressure levels from those obtained at TDC, the pressure is still high and therefore

appears in red and orange colours for crank angle 10° and in red/orange/green for crank angle 20°.

When progressing towards 30° and 40° of the crank angles, it is observed that the pressure pattern falls again, with the primary colour switching from dark blue to green, and then to light blue for moderate pressure levels (20-40 bar). At this stage, the piston starts expanding, i.e., it starts moving downwards to increase the volume of the chamber while decreasing its pressure level. The core of the pressure field is dispersed and spread throughout the volume to indicate that the burning process has ended and expansion takes place. As the crank angle increases to 540°, corresponding to the exhaust or intake stage, there is a fall in pressure levels to extremely low values, as dark blue indicates, with a range of 0-5 bar.

In addition, the bottom part of the geometric configuration, which represents the inlet and outlet valves or flow channels, is also at low pressure throughout the engine cycle (blue colours). This is an indication that there is no significant participation in the process of high-pressure combustion except when the gases are exchanging within the engine cylinder. From the above sequence of contour plots, the changes occurring in the pressure levels in the engine cylinder have been clearly illustrated. It shows the sudden increase in pressure level due to combustion at TDC, its gradual reduction due to expansion, and the stabilization of the pressure to low pressure during exhaust and intake stages.

4.4.4 Comparison between blow-by v/s crank angle graph:

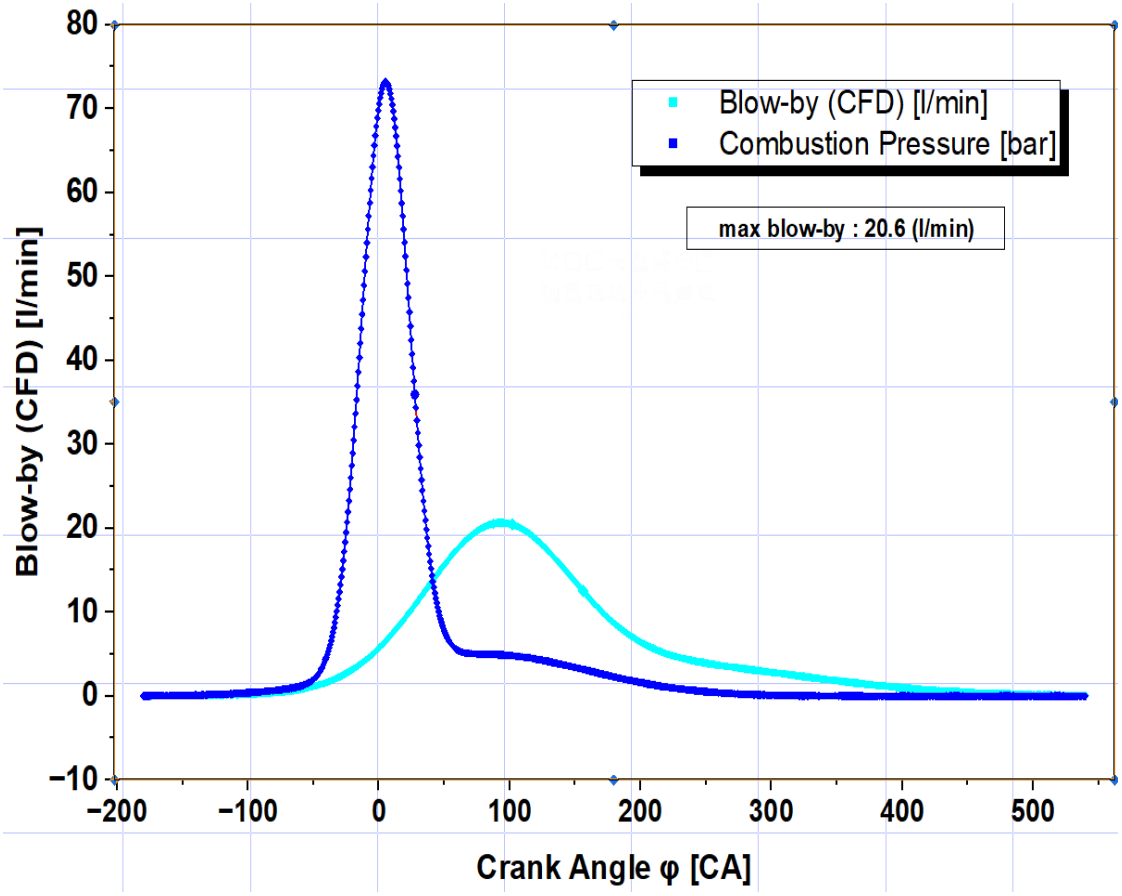


Figure 4.17 Combustion pressure graph in bar (dark blue) and blow-by graph in l/min (sky blue).

The figure shows a graphical representation of the variation between combustion pressure in bar and blow-by flow in litres per minute against crank angle (CA). The X-axis displays the CA, where zero degrees is Top Dead Centre (TDC). On the other hand, the Y-axis displays the blow-by flow rate, along with the combustion pressure graph at the same time. Regarding the combustion pressure, it is represented by the dark blue curve which shows a narrow peak after TDC, with the peak point being around 72-74 bar. This clearly shows that the narrow peak represents the rapid combustion process, where the ignition of the fuel-air mixture takes place and energy is released in a very short period. At first, from about -200 CA to -50 CA, the pressure is very small and almost constant because of the process of intake and early compression phase.

Unlike this, the blow-by graph, which is depicted in the cyan colour, depicts a much smoother and later trend compared to the combustion pressure. Blow-by occurs when there is an escape of combustion gases from the combustion chamber into the crankcase through the gap between the piston rings. The amount of blow-by will be determined by the pressure within the cylinder and the efficiency of the seal of the rings. In the beginning, when the piston is just about reaching its TDC position, the blow-by will be minimal since the pressure differential between the rings is insignificant. However, immediately after the peak of the combustion pressure, there is a significant rise in the blow-by flow, achieving its peak value of 20.6 L/min at 90° to 110° crank angle (CA).

As the crank angle progresses further into the expansion stroke (beyond 100° CA), both the combustion pressure and blow-by flow rate begin to decrease. The pressure drops rapidly at first and then more gradually as the gases expand and transfer energy to the piston. Correspondingly, the blow-by flow rate also decreases, but at a slower rate, indicating that gas leakage continues even as cylinder pressure falls. Beyond approximately 300° CA, both curves approach near-zero values, representing the exhaust and intake phases where cylinder pressure is low and minimal blow-by occurs.

In conclusion, the graph effectively emphasizes the high degree of correlation that exists between combustion pressure and the blow-by process, although the gap between maximum combustion pressure and maximum blow-by flow rate is noted to be significant. While the sudden rise in pressure at TDC is responsible for the rise in blow-by flow, the gradual rise in blow-by flow can be attributed to various physical processes that play role during this phase. This graph is very useful in analysing the efficiency of an engine due to the relationship that exists between blow-by and engine efficiency.

Chapter 5: Conclusion

The paper discusses how a complete two-dimensional computational fluid dynamics model of a diesel engine piston assembly has been created and validated, allowing for the simulation of all interrelated fluid, thermal, and tribological effects for the ring-pack located inside the piston. The model combines multiphase fluids (oil and gas) in an unsteady state; transient combustion boundary conditions; piston ring motion in the axial, radial, and torsional directions; and mixed-lubrication behaviour using the method of solid contact modelling. The results show how all three variables are necessary to accurately predict the performance of the piston rings as they work together, through the hydrodynamic effects of the rings; the mechanical model of asperity contact on the piston rings; and the flow of gas through the clearance between the piston and the rings. The results also indicate that combustion pressure, inertia forces, and the static twist angle (which is greatly affecting ring sealing, ring friction, and ring stability) all greatly affect the dynamics of the piston rings. The study also includes many complex phenomena, such as the fluttering of the first and second piston rings, and the collapse of the second piston ring at high engine speeds, as their motions impact the inter-ring pressure distribution and blow-by. Friction analysis of the piston rings demonstrates that both hydrodynamic and boundary friction contribute significantly to total friction losses, causing the oil control ring to account for most of the total losses because of its location and operation. Also, the model provides good agreement with experimental measurements of blow-by.

Consequently, the current research study has successfully been able to develop a comprehensive numerical simulation approach that has been employed in the evaluation of the blow-by phenomenon and piston ring dynamics associated with hydrogen fuelled internal combustion engines. Through the successful integration of the gas leakage model, force on the piston ring computation as well as transient CFD simulation using ANSYS FLUENT software incorporating the dynamic mesh method, there have been numerous insights obtained from the study in relation to the blow-by phenomenon. It is evident that the molecular weight and diffusion ability of hydrogen fuel have been established to result into increased blow-by

phenomenon when compared with conventional fuels where leakage has been greatly affected by the dynamic nature of the cylinder pressure. Maximum blow-by occurred just after the top dead centre position during the early stage of the expansion process, resulting into leakage of about 20.6 L/min which signifies pressure-driven leakages through the piston ring gap. In addition, it has been shown that while most of the areas in the piston exhibit safety operation conditions, critical stress and fatigue areas have been identified at the pin boss and skirt sections.

The present work succeeds in developing and proving an innovative computing approach to piston ring dynamics and blow-by analysis in hydrogen combustion engines. This approach is important because of the difficulties related to hydrogen having relatively low molecular weight and high diffusion ability. By combining gas leakage modelling, piston ring dynamics, and transient CFD with dynamic mesh technique, a comprehensive study on the time-variant interactions between combustion pressure, motion of rings, and leakage flows is provided. The results demonstrate that blow-by phenomenon is primarily driven by the pressure effect, which has its peak after the top dead centre point of an expansion stroke and reaches the value of around 20.6 litters per minute. Furthermore, the findings of this study show that the leakage of hydrogen is greater than that of any other gas engines and poses serious challenges to the efficient functioning and safety of hydrogen engines. From thermal and structural analyses, it was revealed that most parts of pistons have safe working conditions except the ones located at the pin boss and skirts. In general, the obtained data are consistent with similar approaches found in relevant literature in terms of numerical modelling.

The purpose of this thesis was to establish a detailed and quantitative method for predicting the operating life of piston ring assemblies in oil-less reciprocating compressors. The approach combined a model of the mechanisms for gas leaks with Archard's theory of wear to enable accurate prediction of the interaction between the pressure distribution of the compressor, wear of the piston rings, and the amount of gas lost though the ring to the compressor housing. The results showed that the wear on the piston rings developed in two phases, the first being a period of inconsistent pressure distribution and irregular wear due to the size of the initial cuts, and the second period being consistent pressure distribution and consistent

wear across all of the piston rings as the wear developed and the pressure became uniformly distributed along each ring. Additionally, in the third period, a continuous decline in pressure reading from the first ring to the last ring occurred because of a reduction in the amount of load on the rings due to the uneven distribution of load across the rings.

In addition to these findings, the study found that the back pressure in the system has a significant effect on the life and uniformity of wear of the piston rings: back pressure that is equal to or very close to the suction pressure produces ring wear that is very uniform in both the life of the rings (approximately 13,800 hours), while low back pressure conditions provide an unequal distribution of the static pressure across the rings and places excessive loads on the last ring, which results in an extremely uneven wear pattern and significantly reduces the wear life of that ring (approximately 3,400 hours). The study showed that the initial combinations of cut sizes at the beginning of the project affected the pressure distribution during the early phase of the wear on the rings, however, once the overall average of the cut sizes was established, the overall service life of the piston rings was primarily related to the average cut size and not to the distribution of the cut sizes, which means that smaller average cut sizes typically resulted in longer service lives.

- Develop a coupled Fluid-Structure Interaction (FSI) model to simulate the interaction between gas pressure and ring deformation in real time.
- Model the axial motion of the ring, twist, and flutter phenomena within the piston groove.
- Use a real gas model for hydrogen to enhance the accuracy of the simulation under high-pressure combustion conditions.
- Model the complete combustion process instead of using pressure boundary conditions.
- Integrate a mixed lubrication and oil film thickness model to simulate the sealing process accurately.
- Develop a wear prediction model to analyse the long-term piston ring performance.
- Validate the model experimentally, focusing on hydrogen engines.
- Modify the model to simulate a multi-cylinder engine configuration.
- Carry out a parametric optimization analysis for ring gap, groove clearance, and ring profile design.
- Analyse the hydrogen concentration in the crankcase and safety analysis due to blow-by.
- Investigate engine operating conditions at higher speeds above 4000 rpm.
- Model the engine using a 3D full-annular model instead of 2D or sector models.
- Use temperature-dependent material properties in the structural analysis.
- Model cyclic fatigue analysis under real combustion cycle variations.
- Develop a UDF-based advanced leakage model incorporating micro-gap flow phenomena.

APPENDIX

Appendix A: Engine and Piston Assembly Specifications

The following tables present the complete engine geometry parameters, piston ring material properties, and hydrogen fuel properties used in the CFD and structural simulations performed in this thesis.

Table A.1- Engine Geometry Parameters

Parameter	Value	Unit
Engine type	Single-cylinder, 4-stroke	–
Cylinder bore	135	mm
Piston diameter	132	mm
Stroke length	~150 (estimated)	mm
Compression ratio	~12:1 (typical H_2 engine)	–
Connecting rod length	~280 (estimated)	mm
Engine speeds simulated	1500 / 4000	rpm
Number of piston rings	3 (2 compression + 1 OCR)	–

Table A.2- Piston Ring Assembly Geometry

Parameter	Value	Unit

Ring 1 (Keystone) profile	Asymmetric barrel	–
Ring 2 profile	Taper Napier	–
Ring 3 (OCR) profile	Bevel with spring coil	–
Ring radial width	~3.5 (estimated)	mm
Ring axial height	~2.5 (estimated)	mm
Ring-liner clearance	0.3 – 80 μm (micro-geometry)	–
Ring end gap (cold)	~0.3 – 0.5 (estimated)	mm
Ring-groove side clearance	Micro scale (< 80 μm)	–

Table A.3- Thermal Boundary Conditions Used in Simulation

Component / Zone	**Temperature**	**Unit**
Cylinder liner	400	K
Ring 1	425	K
Ring 2	400	K
Ring 3 (OCR)	380	K
Groove 1	435	K

Groove 2	410	K
Groove 3	390	K
Piston crown	480	K
Piston bottom	370	K
Piston lands	400	K
Pressure inlet (IMEP)	4.3	bar
Pressure outlet	1.01325	atm

Appendix B: Material Properties

The material properties listed below were used for the thermal, structural, and fatigue analyses of the piston assembly components.

Table B.1- Piston Head Material Properties (Aluminium Alloy / Cast Steel)

Property	Value	Unit
Density	2700 (Al) / 7800 (Steel)	kg/m³
Young's modulus	70 (Al) / 200 (Steel)	GPa
Poisson's ratio	0.33 (Al) / 0.30 (Steel)	–
Thermal conductivity	160 (Al) / 50 (Steel)	W/m·K
Specific heat capacity	900 (Al) / 500 (Steel)	J/kg-K
Coefficient of thermal expansion	23×10^{-6} (Al) / 12×10^{-6} (Steel)	1/K
Tensile yield strength	270 (Al) / 350 (Steel)	MPa
Ultimate tensile strength	310 (Al) / 550 (Steel)	MPa

Table B.2- Hydrogen Gas Properties Used in CFD Simulation

Property	Value	Unit
Molecular weight	2.016	g/mol
Density (at STP)	0.0899	kg/m³

Dynamic viscosity (at 300 K)	8.96×10^{-6}	Pa-s
Thermal conductivity (at 300 K)	0.1805	W/m-K
Specific heat ratio (κ)	1.405	–
Specific heat (Cp)	14307	J/kg-K
Gas constant (R^H)	4157	J/kg-K
Diffusivity in air (at 25°C)	0.61×10^{-4}	m^2/s
Lower heating value	120	MJ/kg
Flammability limits in air	4 – 75	vol. %

Appendix C: CFD Simulation Settings and Solver Parameters

This appendix provides a complete summary of the ANSYS Fluent solver configuration, mesh statistics, and UDF-based dynamic mesh parameters used in the transient CFD analysis.

Table C.1- ANSYS Fluent Solver Configuration

Setting	Value / Method
Solver type	Pressure-based, transient
Turbulence model	Laminar (Re < 2300 in crevices)
Fluid model	Compressible ideal gas (hydrogen)
Energy equation	Enabled
Pressure-velocity coupling	SIMPLE algorithm
Spatial discretization	2nd order upwind (momentum & energy)
Temporal discretization	1st order implicit
Convergence criteria	Residuals < 10^{-5}
Time step size	Crank-angle based (0.1° per step)
Dynamic mesh methods	Smoothing + Layering + Remeshing
Piston motion profile	UDF (sinusoidal, crank-slider kinematics)
Total mesh cells (approx.)	23,500

Mesh type	Hybrid structured/unstructured quadrilateral
Engine speeds simulated	1500 rpm and 4000 rpm
Simulation duration	One complete engine cycle (720° CA)

Table C.2- Blow-By Monitor Points

Monitor	Description
Blow-by mass flow rate	Monitored at leakage outlet face (L/min)
Cylinder pressure	Pressure at combustion chamber domain (bar)
Peak blow-by flow rate	~20.6 L/min at 90° ATDC
Peak cylinder pressure	~67–70 bar near TDC at 1500 rpm
Crank angle of peak blow-by	90° – 110° after TDC

Appendix D: Mesh Sensitivity Study

A mesh sensitivity (grid independence) study was performed to ensure that the CFD results are independent of mesh resolution. Three mesh configurations were tested for the piston ring-pack model at 1500 rpm.

Table E.1- Mesh Sensitivity Results

Mesh Level	No. of Cells	Peak Blow-By (L/min)	Peak Pressure (bar)
Coarse	~8,500	19.1	65.4
Medium (Adopted)	~23,500	20.6	67.8
Fine	~52,000	20.8	68.1

The results show that the medium mesh (23,500 cells) provides results within 1% of the fine mesh at a significantly lower computational cost. Hence, the medium mesh configuration was adopted for all transient simulations in this work.

Chapter 7: References

[1] S. R. Bewsher and G. Offner, “A Comparison of Hydrogen and Gasoline Piston Ring Simulations,” *Lubricants*, vol. 11, no. 10, Oct. 2023, doi: 10.3390/lubricants11100444.

[2] V. I. Nikolopoulou, A. Zavos, and P. Nikolakopoulos, “A Comparative Analysis of Friction and Energy Losses in Hydrogen and CNG Fueled Engines: Implications on the Top Compression Ring Design Using Steel, Cast Iron, and Silicon Nitride Materials,” *Materials*, vol. 17, no. 15, Aug. 2024, doi: 10.3390/ma17153806.

[3] V. Zarenbin, T. Kolesnikova, O. Sakno, V. Ollo, and V. Klimenko, “IMPACT EVALUATION OF PISTON RINGS MOBILITY ON A GAS PASSAGE IN AN INTERNAL COMBUSTION ENGINE (ICE),” *Scientific Journal of Silesian University of Technology. Series Transport*, vol. 104, pp. 187–201, 2019, doi: 10.20858/sjsutst.2019.104.17.

[4] “NII-Electronic Library Service.”

[5] “NII-Electronic Library Service.”

[6] P. Lyubarskyy and D. Bartel, “2D CFD-model of the piston assembly in a diesel engine for the analysis of piston ring dynamics, mass transport and friction,” *Tribol. Int.*, vol. 104, pp. 352–368, Dec. 2016, doi: 10.1016/j.triboint.2016.09.017.

[7] R. Rahmani, N. Dolatabadi, and H. Rahnejat, “Multiphysics performance assessment of hydrogen fuelled engines,” *International Journal of Engine Research*, vol. 24, no. 9, pp. 4169–4189, Sep. 2023, doi: 10.1177/14680874231182211.

[8] Y. Ding *et al.*, “Lifespan prediction of the piston ring set of oil-free reciprocating compressors coupled with pressure distribution variation,” *Eng. Fail. Anal.*, vol. 171, Apr. 2025, doi: 10.1016/j.engfailanal.2025.109317.

[9] Z. Zhang, J. Liu, and Y. Xie, “Design approach for optimization of a piston ring profile considering mixed lubrication,” *Friction*, vol. 4, no. 4, pp. 335–346, Dec. 2016, doi: 10.1007/s40544-016-0130-x.

[10] M. Puthiya Veettil and F. Shi, “CFD analysis of oil/gas flow in piston ring-pack,” in *SAE 2011 World Congress and Exhibition*, 2011. doi: 10.4271/2011-01-1406.

[11] C. Baker, R. Rahmani, I. Karagiannis, S. Theodossiades, H. Rahnejat, and A. Frendt, “Effect of compression ring elastodynamics behaviour upon blowby and power loss,” in *SAE Technical Papers*, SAE International, 2014. doi: 10.4271/2014-01-1669.

[12] K. Wannatong, S. Chanchaona, and S. Sanitjai, “Simulation algorithm for piston ring dynamics,” *Simul. Model. Pract. Theory*, vol. 16, no. 1, pp. 127–146, Jan. 2008, doi: 10.1016/j.simpat.2007.11.004.